Laser-assisted Delivery of Topical Methotrexate

- *In vitro* investigations

Elisabeth Hjardem Taudorf

This review has been accepted as a thesis together with three previously published papers by University of Copenhagen February 11, 2016 and defended April 14, 2016

Tutors: Merete Hædersdal, Rox Andersson, Uwe Paasch, and Catharina M Lerche

Official opponents: Albert Wolkerstorfer and Peter Bjerring

Correspondence: Elisabeth Hjardem Taudorf, Dpt. of Dermatology, Bispebjerg University Hospital, Bispebjerg Bakke 23, 2400 Copenhagen NV, Denmark

E-mail: Ehtaudorf@dadlnet.dk

Dan Med J 2016;63(6):B5254

LIST OF STUDIES

Taudorf EH, Haak CS, Erlendsson AM, Philipsen PA, Anderson RR, Paasch U, Haedersdal M. Fractional ablative erbium YAG laser: histological characterization of relationships between laser settings and micropore dimensions. Lasers Surg Med. 2014 Apr; 46 (4):281-9. Epub 2014 Feb 5.

Taudorf EH, Lerche CM, Erlendsson AM, Philipsen PA, Hansen SH, Janfelt C, Paasch U, Anderson RR, Hædersdal M. Fractional laser-assisted drug delivery: Laser channel depth influences biodistribution and skin deposition of Methotrexate. Lasers Surg Med. 2016 Feb 5. [Epub ahead of print]

Taudorf EH, Lerche CM, Vissing AC, Philipsen PA, Hannibal J, D'Alvise JT, Hansen SH, Janfelt C, Paasch U, Anderson RR, Hædersdal M. Topically applied Methotrexate is rapidly delivered into skin by fractional laser ablation. Expert Opin Drug Deliv. 2015 Jul;12(7). Epub 2015 Apr 20:1-11.

BACKGROUND

Topical drug delivery across skin barrier

The skin imposes a physico-chemical barrier to topical drug delivery. Pretreatment with various chemical or physical techniques can disrupt skin barrier and enable enhanced delivery of well-known topical drugs as well as new possibilities for topical application of systemic drugs. Thus, pretreatment of the skin may enhance the efficacy of topical treatments as well as broaden the spectrum of available topical drugs. Some barrier disruption techniques may even facilitate customized treatments targeted at dermatological diseases in specific layers of the skin. Furthermore, systemic exposure can potentially be avoided in localized dermatological diseases, whereby adverse effects from systemic therapy may be minimized.

Skin is composed of an epidermis and a dermis with appendages such as hair follicles, sweat glands and sebaceous glands. The superficial unviable stratum corneum consists of keratin-filled dead corneocytes with low water content, whereas the underlying viable parts of epidermis contain keratinocytes with a high water content [1, 2]. Stratum corneum consists of 15 – 20 layers of densely packed corneocytes surrounded by an extracellular matrix of hydrophobic non-polar lipids in a "brick-and-mortar" structure that protects underlying tissue from mechanical stress, dehydration, infectious agents and chemicals [3]. Stratum corneum is considered the main barrier for topical drug delivery [1–3] although studies have also demonstrated barrier function of the basement membrane and of tight junctions between keratinocytes in viable epidermis [4, 5]. Passive absorption across the unviable stratum corneum into underlying viable epidermis and dermis may occur by: i) Transcellular absorption through cell membranes of corneocytes, ii) Intercellular absorption in the lipid matrix surrounding corneocytes and iii) Appendageal absorption through hair follicles and glands [6, 7]. Despite these passageways, absorption into and across skin is impaired for hydrophilic and charged molecules as well as lipophilic molecules of > 500 Da [6, 8, 9].

The rate of drug absorption is described by Fick's law of passive diffusion:

$$\text{Flux} = (P \times D \times \Delta C)/\Delta L$$

Flux increases by higher partitioning of the drug from vehicle into stratum corneum (P = Partitioning coefficient), ability to diffuse within the skin (D = Diffusion coefficient) and difference in drug concentration between vehicle and skin (ΔC = Concentration gradient). In contrast, flux decreases when the diffusion pathway increases (ΔL = Length of the diffusion pathway) [6, 7].

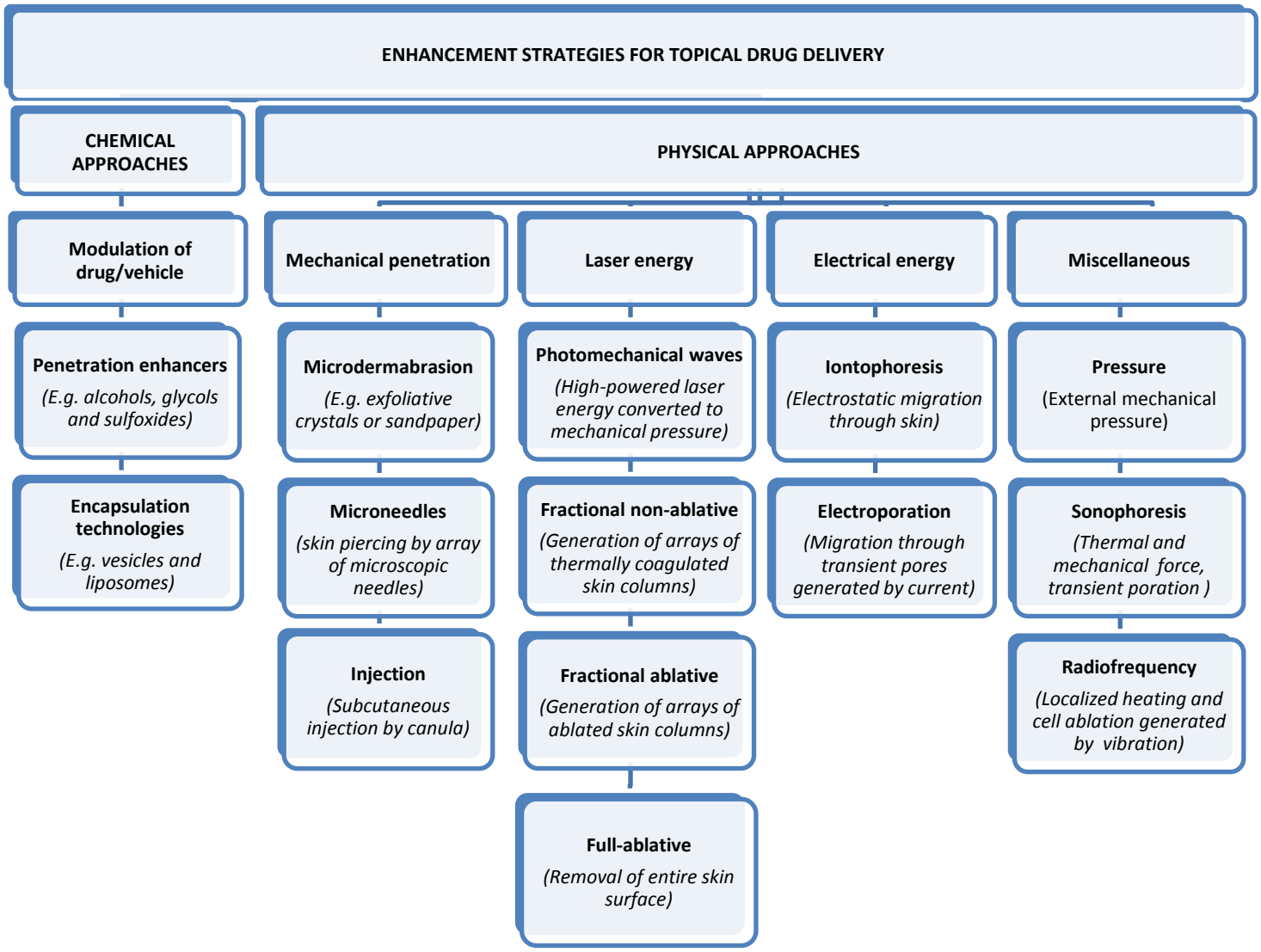

Figure 1: *Enhancement strategies for topical drug delivery. Modified from Schuetz et al., 2005* [10] *and Brown et al., 2006* [9].

Chemical as well as physical approaches have been applied in order to enhance skin permeability and flux of small lipophilic drugs as well as to enable topical delivery of large, hydrophilic or charged molecules as illustrated in fig. 1 [9, 10]. Chemical techniques include penetration enhancers in vehicles or skin patches such as alcohols, glycols and sulphoxides as well as encapsulation of topically applied molecules in e.g. vesicles or liposomes (fig. 1) [11, 12]. Chemical enhancement has the advantage of being noninvasive and often inexpensive, whereas disadvantages include inability to deliver large amounts of drug, difficulty in controlling rate of penetration and risk of contact sensitivity [9, 11, 12]. Physical barrier disruption techniques generally delivers larger amounts of drug than chemical enhancement techniques and include mechanical penetration, laser energy, electrical energy or other energy-based devices (fig. 1). Challenges to the physical techniques may include lack of standardization, difficulty to control rates of penetration and limited ability to target topical drugs at specific layers of the skin. The ablative fractional laser (AFXL) technology offers a possibility to generate standardized laser-tissue interactions and provide a customized and reproducible number of laser channels of precise and adjustable dimensions with minimal ablation of surface area [13]. Variation of laser channel dimensions can be utilized to personalize laser treatments. Penetration depth is of specific clinical interest since it may affect the ability to target laser-assisted drug delivery at specific skin layers. Furthermore, the laser channels of ablated tissue may serve as a reservoir for topical drugs.

In this PhD thesis, AFXL has for the first time been utilized to deliver topical Methotrexate (MTX). Topical skin deposition, biodistribution and transdermal permeation are investigated for up to 24 h of continuous MTX exposure and new knowledge is added regarding impact of penetration depth and transport kinetics on AFXL-assisted topical delivery of MTX.

Laser

The word Laser is an acronym for *L*ight *A*mplification by *S*timulated *E*mission of *R*adiation [14]. A laser emits monochromatic, coherent, unidirectional light through a process of optical amplification based on stimulated emission of electromagnetic radiation [14]. The result is single-wavelength, uni-directional photons moving in-phase in a collimated narrow beam. The beam can

either stay focused over long distances or provide intense energy at specific skin sites.

Available lasers cover a spectrum of ultraviolet, visible and infrared wavelengths [14]. The selected wavelength as well as the energy level of the laser affects depth of penetration, and medical lasers of specific wavelengths typically target distinct tissue chromophores such as e.g. hemoglobin, melanin, hydroxyapatite or water (fig. 2) [15]. When a laser of a certain wavelength, energy and pulse duration is absorbed by a defined chromophore, a controlled destruction is induced without significant damage to the surrounding tissue, as described by the theory of selective photothermolysis [16].

Lasers that target tissue water can be either non-*ablative* or *ablative* depending on the absorption coefficient. *Non-ablative* lasers, as e.g. the neodymium-doped yttrium aluminium garnet laser (1,440nm Nd:YAG) and the erbium glass laser (1,540 nm Er:Glass), have low absorption coefficients in tissue water and cause thermal coagulation in the dermis beneath an intact skin barrier (fig. 2) [14, 15, 17]. *Ablative* lasers have higher absorption in tissue water and evaporates the epidermal skin barrier as well as underlying tissue (fig. 2) [14, 15, 17]. Examples of *ablative* lasers include erbium-doped yttrium scandium gallium garnet laser (2,790 nm YSGG), erbium-doped YAG lasers (2,940 nm Er:YAG), and carbon dioxide lasers (10,600 nm CO_2) (fig. 2). Laser energy can be applied to the entire skin surface or to specific fractions of skin. The concept of non-ablative fractional photothermolysis was invented in 2004 [18], and was further developed into ablative fractional laser (AFXL) in 2007 [13, 19].

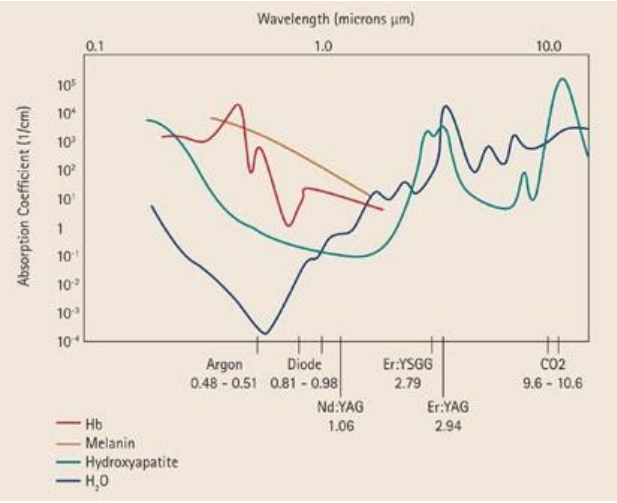

Figure 2: *Absorption spectra of chromophores and related wavelengths of selected medical lasers. The illustrated chromophores are: Hemoglobin (Hb, target in vascular lesions), Melanin (target in pigmented lesions), Hydroxyapatite (target at dental operations), and water (H_2O, target in tissue ablation). Illustration from Parker et al., 2007* [15].

Ablative fractional laser (AFXL)

AFXL physically disrupts the skin barrier and generates arrays of ablated laser channels into the skin, leaving surrounded skin unaffected as illustrated in fig. 3. Each ablated column constitutes a microscopic ablation zone (MAZ) that may be utilized for intra- and transdermal drug delivery (fig. 3) [13, 19]. Ablated MAZ dimensions are described by ablation depth (AD), thickness of the thermal coagulation zone lining the laser channel (CZ) and epidermal ablation width (AW) [20].

Ablative fractional laser holds the potential to provide accurate and reproducible arrays of MAZs that can be adjusted by varying laser parameters. The number of ablated channels can be adjusted by varying surface ablation density, while the dimensions of each ablated MAZ is modulated by the applied laser energy.

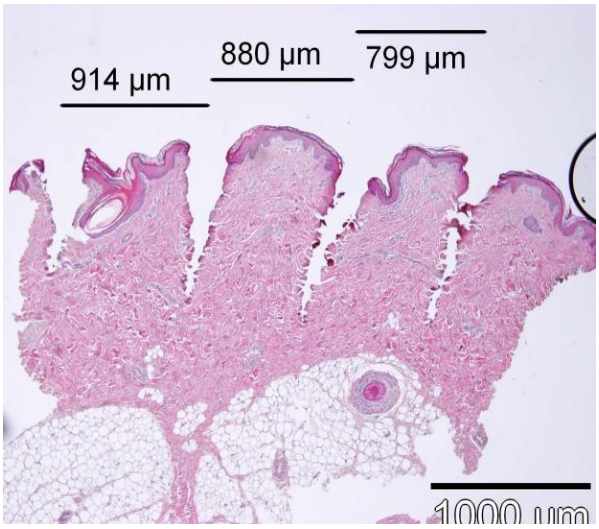

Figure 3: *Cross-section of porcine skin exposed to ablative fractional laser of 5 % density illustrating four ablated columns lined by coagulation zones and surrounding unaffected skin. Haematoxylin & Eosin stained (H&E).*

Surface ablation density is defined as fraction of skin surface covered by MAZs and can typically be adjusted in the range of 1 – 40 % depending on laser device [17]. Density can be calculated theoretically from the spot size of the laser beam or experimentally based on the histologically measured AW of ablated MAZs ($\pi \times (^1/_2 \times AW\ (cm))^2 \times MAZs/cm^2$). In addition, the total ablated skin volume per cm^2 can be experimentally determined based on histologically measured dimensions and the mathematical formula for volume of a cone ($^1/_3 \times \pi \times (^1/_2 \times AW\ (cm))^2 \times AD\ (cm) \times MAZs/cm^2$) [20]. Dimensions of each individual MAZ can be varied by adjusting the physical properties of the delivered energy. The total energy delivered per MAZ (mJ/MAZ) is determined by multiplying pulse energy (mJ/microbeam) with the applied number of stacked pulses. The pulse energy is generated from the available laser power (Watt), and high-powered laser devices thus provide higher pulse energy by fewer stacked pulses to build up total energy than low-powered laser devices. High pulse energies are generally found to generate deeper tissue penetration than low pulse energies [13, 20, 21], whereas the duration of each pulse (μs – ms), as well as the frequency of delivered pulses (Hz) may also affect MAZ dimensions.

Initially, lasers based on large platforms provided high power levels and pulse energies, while lately, small portable fractional lasers utilize stacked pulses to compensate for low pulse energies. Knowledge is sparse on laser-tissue interactions for the large variety of miniaturized lasers with different specifications [17], although the use is increasing due to a growing clinical demand for AFXL treatments and laser-assisted topical drug delivery. Thus, histological MAZ dimensions generated by a miniaturized low-powered Er:YAG AFXL is investigated in this PhD thesis and used as a model of general AFXL in the further studies of AFXL-assisted topical MTX delivery.

Table 1: AFXL-assisted delivery of topically applied agents for selected disorders

Disorder	**Applied agent**	**Reference *(Level of evidence[d])***			
		In vitro	***In vivo animal***	***Human clinical studies***	***Human RCTs[g]***
Actinic Keratosis/ Mb. Bowen/ BCC[c]	MAL[a]		[45] [46] [47] [48]	[23] (IIb) [30] (IIa)	[25] (Ia) [26] (Ia) [27] (Ia) [28] (Ia) [29] (Ia) [32] (Ia) [34] (Ia) [33] (Ia) [42] (Ia)
	ALA[b]	[49, 50]	[47]		
	Ing. Meb.[e]	[51]		[24] (IV)	
	Fluorouracil			[31] (IIb)	
	Imiquimod	[52]	[52]		
	Diclofenac	[53]			
Scars & Keloids	Topical Steroid	[54]		[35] (IIb) [36] (III)	
	PLLA[f]			[37] (IIa)	
Pain	Lidocaine	[55]	[56]		[57] (Ia) [38] (Ia)
Onychomycosis	Amorolfine			[39] (IIb)	
Warts	ALA[b]			[22] (IIb)	
Hemangiomas	Timolol			[40] (IIb)	
Aesthetic treatments	Botulinum toxin				[41] (Ia)
	Vitamin C	[58] [59]	[58]		
	Tranexamic acid	[60]			
Vaccines	Ovalbumin		[61]		
Experimental	Stem cells		[62, 63]		
	Antibodies	[64]	[64]		

[a] *MAL: Methyl aminolevulinate (photosensitizer)*
[b] *ALA: Aminolevulinic acid (photosensitizer)*
[c] *BCC: Basal Cell Carcinomas*
[d] *Level of Evidence* [65]: *Ia: RCT*
IIa: Clinical placebo-controlled study
IIb: Prospective Cohort study
III: Retrospective descriptive study
IV: Case report
[e] *Ing.Meb.: Ingenol Mebutate*
[f] *PLLA: Poly-L-Lactic Acid*

Ablative fractional laser for topical drug delivery

The concept of AFXL-assisted topical drug delivery was introduced in 2009 [22] and has since been profoundly investigated as illustrated in table 1. The technique has been applied for a range of clinical indications including precancerous lesions and non-melanoma skin cancers (NMSC) [23–34], scars and keloids [35–37], anesthetics [38], onychomycosis [39], warts [22], hemangiomas [40] and aesthetic conditions [41] (Table 1). The field of AFXL-assisted topical drug delivery for precancerous lesions and NMSC is thoroughly investigated and promising clinical results have especially been achieved by AFXL-assisted delivery of methyl aminolevulinate (MAL) prior to PDT-treatment of precancerous lesions [23, 25–29, 33, 34, 42] (Table 1). However, complete clearance rates has not been reached for all patients, and especially the treatment of thick nodular Basal Cell Carcinomas (BCCs) [30, 32] and multiple actinic keratoses in immunosuppressed patients can be challenging [26, 29]. Hence, further knowledge is needed on optimal treatment conditions. Topical treatments targeted at tumor cells in superficial as well as deep skin layers may increase clearance rates. Besides, pretreatment by AFXL could extend the spectrum of available anti-cancer drugs to include topical delivery of systemic chemotherapeutic agents.

Methotrexate (MTX)

Methotrexate is a well-proven chemotherapeutic and anti-inflammatory drug [43, 44]. Mechanism of action behind the anti-inflammatory properties of MTX is uncertain, while the anti-neoplastic property is mainly caused by antimetabolite activity. MTX blocks folic acid metabolism and consequently disturbs de novo synthesis of thymidylate and purines, whereby DNA and RNA synthesis is inhibited [44]. MTX is administered by oral or parenteral routes and systemic distribution inflicts a risk of severe adverse effects such as pneumonitis, myelotoxicity and hepatotoxicity [66]. Generalized dermatological inflammatory diseases often benefit from systemic MTX therapy, while topical delivery of MTX may be a safer choice for the treatment of localized dermatological tumors or inflammatory disorders [67]. However, the 454 Da, hydrophilic MTX-molecule (log P = – 1.85), which is negatively charged at physiological pH, has negligible capacity for passive diffusion across the intact skin barrier [44, 67]. Thus, the molecule can be considered a model for other hydrophilic or charged molecules, which cannot penetrate skin barrier. Pretreatment by AFXL has not previously been utilized to deliver topical MTX, while previous *in vitro* studies have demonstrated that MTX is capable of penetrating the skin barrier by chemical enhancement [68–71], iontophoresis [72–77], electroporation [78], microneedles [72, 79], and full-ablative laser exposure [78].

Studying topical drug delivery *In vitro*

In vitro diffusion of topical drugs is studied in *vertical* upright or in *horizontal* side-by-side test chambers with static or continuously replaced "flow-through" receiver fluid [7, 80]. *Vertical* diffusion cells are preferred for studies of semi-solid formulations, while both types can be used to study diffusion of aqueous solutions [7, 80]. A "flow-through" receiver fluid and a viable skin membrane are required to study the effect of skin metabolism on drug absorption, while specific information about drug diffusion can be obtained by nonviable skin in static diffusion cells. The most commonly used *vertical* type of static diffusion cells, the Franz skin permeability cells (FC), was selected in this PhD thesis to study AFXL-assisted topical delivery of aqueous MTX-disodium solution (fig. 4).

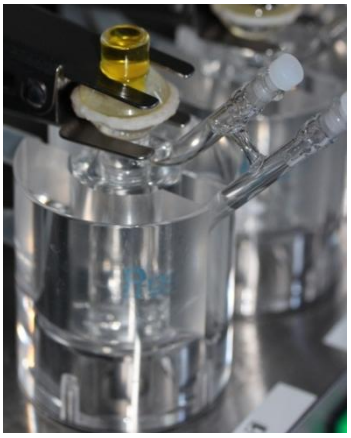

Figure 4: *Franz skin permeability Cells: Donor chamber filled with 1.0 ml yellow MTX solution and receiver chamber filled with 5.5 ml static uncolored Phosphate buffered saline (PBS), divided by porcine skin membrane.*

Donor chamber

Drugs can be exposed to the donor chamber in *finite* or *infinite* doses [7]. *Finite* doses are absorbed almost totally from donor chambers during experiments, and are suitable to study rate of absorption and maximum amount of absorption. In contrast, *infinite* doses, typically of more than 10 mg/cm^2 as selected in the present PhD thesis, can be maintained throughout experiments and enable studies at steady-state conditions of maximum absorptions rates and cumulative absorption over time [7, 81]. Exposure time in the donor chamber should ideally reflect the relevant clinical application time. Yet, exposure beyond 24 h should be avoided due to risk of skin membrane deterioration [7, 82]. Other factors that may influence absorption of drug from donor chamber include selected vehicle and physico-chemical properties of the drug, such as molecular weight, polarity, ionization and binding properties [7].

Skin membrane – porcine vs. human

Human skin is considered as golden standard for diffusion studies, while animal skin such as mouse, rat or porcine skin is frequently used due to comparability to other studies, ethic regulations or accessibility [55, 78, 83]. Porcine skin is the best alternative to human skin for *in vitro* studies and was chosen for investigations in this PhD thesis [84]. Porcine skin has high functional, chemical and anatomical resemblance to human skin and is one of the most predictable and stable models for diffusion in humans [7, 55, 84–86]. Permeability coefficients for human and porcine skin are highly correlated, and structural similarities include thick and well differentiated epidermis, sparse hair coat, hairs and infundibula extending deeply into the dermis as well as similar collagen fiber arrangement, content of elastic fibers and vascular anatomy in the dermis [84, 86] (fig. 5). Differences include a slightly thicker stratum corneum in pig skin (20 – 26 µm) than in human skin (11 – 15 µm) and minor chemical distinctions [84, 85, 87] (fig. 5). Skin membranes for diffusion studies can be prepared as full-thickness skin, dermatomed skin removed of deep dermis, or epidermal membranes [82]. In this PhD thesis, full-thickness skin was used, since MAZs reached down to mid-dermal skin layers and diffusion into and across the entire skin membrane was investigated. Skin permeability can vary with temperature,

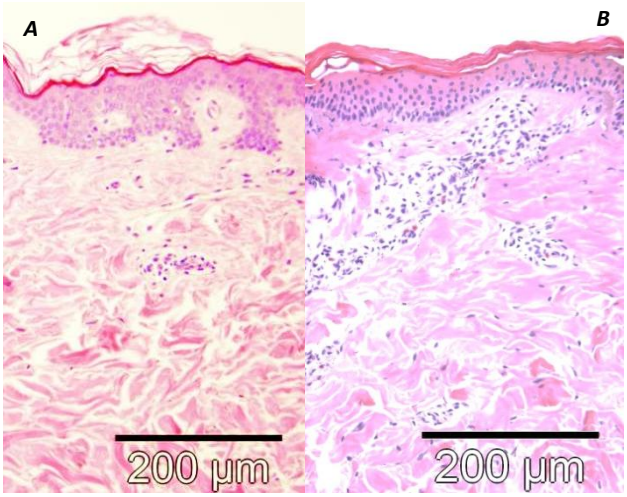

Figure 5: *Haematoxylin & Eosin (H&E) stained skin from human (A) and porcine (B) flank area. Similarities include sparse hair coat and well differentiated epidermal layers while differences include slightly thicker stratum corneum and less differentiated rete ridges in porcine skin.*

hydration, thickness, anatomical site and condition of the skin, and thus, all these parameters should be standardized [7]. Skin barrier integrity should be controlled after preparation and prior to drug diffusion by e.g. measurements of trans-epidermal water loss or by transcutaneous electrical impedance as selected in this PhD thesis [82, 88].

Receiver chamber

The investigated test molecules or drugs should be completely soluble in the receiver solution in order to avoid introduction of false barriers to drug diffusion during FC experiments. Thus, isotonic phosphate buffered saline (PBS) could be used for investigations of hydrophilic molecules, as selected in this PhD thesis, while lipophilic molecules require solvents that increase lipophilicity such as e.g. an ethanol:water mixture [7]. Regardless of selected receiver fluid, composition should not affect skin barrier integrity [81]. In general, protease inhibitors, antiseptic or antibiotic agents may be added to the buffer solution to reduce overgrowth of bacteria or fungus, and to protect fragile test molecules or drugs.

Detection methods

Validated detection methods are essential to describe diffusion of drug into and across skin. For *quantification*, techniques such as radiolabeling of test molecules or drugs, High Performance Liquid Chromatography (HPLC), gas chromatography, or

Table 2: Biodistribution in skin of AFXL-assisted topically applied agents

Imaging technique	Images of	Applied agent	Samples/interv. *n*	Calculations	References
Brightfield microscopy	Dye	Methylene Blue	6	+	[61]
		Sulforhodamine B	1	-	[61]
Widefield fluorescence microscopy	Fluorescent dye	Sulforhodamine B	6	+	[61]
	Fluorescence-labeled molecule	Ovalbumin	6	+	[61]
		Thymoglobulin	1	-	[64]
	Protoporphyrin IX fluorescence	MAL[a]	10	+	[45]
		MAL[a]	10	+	[46]
		MAL[a], ALA[b]	7	+	[47]
		MAL[a]	10	+	[48]
Confocal fluorescence Microscopy	Fluorescent dye	FITZ[c]	1	-	[55]
		FITZ[c]	1	-	[52]
	Fluorescence-labeled molecule	Ovalbumin	3	-	[61]
		Bovine Serum Albumin	1	-	[93]
		P-2[d], FD-4[e], FD-150[e]	1	-	[52]
	Protoporphyrin IX fluorescence	ALA[b]	1	-	[49]

[a] *MAL: Methyl aminolevulinate* [b] *ALA: Aminolevulinic acid* [c] *FITZ: Fluorescein isothiocyanate*
[d] *P-2: Polypeptide with a molecular weight of 2.19 kDa* [e] *FD: Fitz-labeled dextrans of 4 and 150 kDa*

Liquid Chromatography Mass Spectrometry (LC-MS) can be used [7]. MTX has previously been quantified by HPLC [89–91], LC-MS [91], Enzyme-Linked Immunosorbent Assays (ELISA) [90] and spectrophotometry [92]. Apart from quantifying intradermal and transdermal amounts of test molecule or drug it is important to gain knowledge of *qualitative biodistribution* within the skin. Intradermal biodistribution of MTX has never previously been investigated and knowledge of accumulation in specific structures or layers of the skin may lead to the development of improved topical delivery targeted at specific dermatological disorders. As illustrated in table 2, biodistribution of other AFXL-assisted topically delivered test molecules or drugs has so far been imaged by brightfield microscopy [61], widefield fluorescence microscopy [45–48, 61, 64] and confocal fluorescence microscopy [49, 52, 55, 61, 93]. In addition to imaging, quantification or semi-quantification of test molecule or drug concentrations at specific skin levels have been utilized to describe intradermal biodistribution profiles [45–48, 51, 61].

AIM

The overall aim was to characterize AFXL-assisted topical delivery of MTX into and across skin.

Specific study objectives were to investigate:

1. Specific laser-tissue interactions by histological examination and mathematical modeling of MAZ dimensions generated by a miniaturized low-powered Er:YAG AFXL using stacked pulses with a variety of laser settings (*study I*).
2. The impact of specific MAZ depths on AFXL-assisted topical delivery of MTX (*study II*).
3. The importance of transport kinetics to intradermal biodistribution and transdermal permeation of MTX after AFXL-assisted topical delivery (*study III*).

MATERIALS AND METHODS

Study designs

In *Study I,* laser-tissue interactions were characterized in a histological *in vitro* pig skin model (Table 3). Results enabled estimates of specific MAZ dimensions from combinations of laser parameters that were utilized in *studies II* and *III* to investigate the impact of MAZ depth and transport kinetics on topical delivery of MTX in *in vitro* FCs (Table 4).

Fractional laser ablation

A 2,940 nm Er:YAG laser prototype with an internal scanner and a fixed spot size of 225 µm was used in all three studies (P.L.E.A.S.E.® (Precise Laser Epidermal System) Professional, Pantec Biosolutions AG, Ruggell, Liechtenstein). The laser device delivered energy at predefined fixed combinations of power, pulse energy, pulse duration and pulse repetition rate.

In *study I*, A total of 12 laser interventions were evaluated, consisting of four fixed combinations of laser parameters applied by 2, 20 and 50 stacked pulses (Setting 0 – 3, Table 3). Surface ablation density of 5 % (calculated based on spot size) corresponding to 97 MAZs/cm^2 was selected to ensure a sufficient number of MAZs for evaluation in each histological section.

Table 3: Design of study I

Setting	Laser parameters	Stacked pulses	Total Energy (mJ/MAZ)	Biopsies
0	**2.3 mJ/pulse, 1.15 W, 50 µs 500 Hz**	2	4.6	-
		20	46.0	-
		50	115.0	6
1	**5.6 mJ/pulse, 1.69W, 125 µs 300 Hz**	2[MAZ-E]	11.2	6
		20	112.0	6
		50	280.0	6
2	**7.4 mJ/pulse, 2.22W, 225 µs 300 Hz**	2	14.8	12
		20	148.0	10
		50	370.0	11
3	**12.8 mJ/pulse, 1.28 W, 225 µs 100 Hz**	2[MAZ-DS]	25.6	10
		20[MAZ-DM]	256.0	12
		50	640.0	12
Total number of biopsies evaluated				**91**

Settings are categorized according to increasing pulse energy. Pulse energy of 2.3 mJ/pulse did not create histologically visible MAZs at 2 and 20 stacks, and was referred to as setting 0.
MAZ-E: Epidermal Microscopic Ablation Zone (MAZ) *MAZ-DS: Superficial dermal MAZs*
MAZ-DM: Mid-dermal MAZs *Table modified from study I.*

In *study II*, the impact of MAZ depth was studied by MAZs reaching epidermis (MAZ-E), superficial dermis (MAZ-DS) and mid-dermis (MAZ-DM) (Tables 3 and 4), while in *study III*, MAZ-DM were selected for investigation of transport kinetics of topically applied MTX. In both studies, surface ablation density was reduced to 2.4 % (calculated based on spot size) corresponding to 47 MAZs/cm^2. Low density has previously proven sufficient to deliver other topical drugs [45, 51, 94], and was found appropriate for delivery of MTX in pilot studies (not shown).

Porcine skin model

Nonviable porcine flank skin was harvested immediately after euthanasia of female, Danish landrace/Yorkshire pigs (3 months old, 35 – 40 kg). Skin was preserved at -20˚ Celsius (C) for one week (*study I*) or -80˚ C for up to three months (*study II & III*) due to longer duration of FC studies than of histological study. Laser was exposed to clean and dry 20 – 21 ˚C full-thickness skin trimmed of excessive hair. After laser exposure, either five mm punch biopsies were collected and fixated in 4 % paraformaldehyde for histological analyses (*study I*) or skin were transferred to FC chambers for studies of diffusion of MTX (*study II & III*).

Histological evaluation of skin biopsies

Biopsies for histological evaluation of MAZ dimensions were embedded in paraffin, cut vertically in 4 - 6 µm slices, stained with H & E, and evaluated with a bright field microscope equipped with calibrated CellF software (BX41, Olympus, Hamburg, Germany). Based on histological MAZ dimensions found in *study I*, MAZ-E, MAZ-DS and MAZ-DM were selected for analyses of impact of MAZ depth on topical MTX delivery (*study II*), while MAZ-DM was

Table 4: Franz Skin Permeability Cell (FC) study designs (Study II & III)

Study	# of FCs (n = 154)	Dismount time (h)	Samples	Intervention (n= 6 FCs per intervention)								Measuring techniques		
				[a]MTX +				[b]PBS +						
				[c]MAZ-E	[d]MAZ-DS	[e]MAZ-DM	Intact Control skin	[c]MAZ-E	[d]MAZ-DS	[e]MAZ-DM	Intact Control skin	[f]HPLC	[g]FM	[h]DESI-MSI
II	36	21	Donor Receiver Full-skin	x	x	x	x[i]			x	x	x		
	36	21	Skin sections at: • 100 µm • 200 µm • 500 µm • 800 µm • 1200 µm	x	x	x	x			x	x	x		
	48	21	Skin sections at: • 100 µm • 500 µm • 1200 µm	x	x	x	x[j]	x	x	x[j]	x		x	
III	30	0.25; 1.5; 7; 18; 24	Donor Receiver Skin sections at: • 500 µm			x						x	x	
	4	24	Skin sections at: • 500 µm			x	x			x	x			x

[a] *MTX: Methotrexate* [b] *PBS: Phosphate Buffered Saline*

[c] *MAZ-E: Epidermal Microscopic Ablation Zone generated by: 1.69 W, 11.2 mJ/MAZ, 2 stacked pulses, 5.6 mJ/pulse, 125 µs and 300 Hz*

[d] *MAZ-DS: Superficial dermal MAZs generated by: 1.28 W, 25.6 mJ/MAZ, 2 stacked pulses, 12.8 mJ/pulse, 225 µs and 100 Hz*

[e] *MAZ-DM: Mid-dermal MAZs generated by: 1.28 W, 256.0 mJ/MAZ, 20 stacked pulses, 12.8 mJ/pulse, 225 µs and 100 Hz*

[f] *HPLC: High Performance Liquid Chromatography*

[g] *FM: Fluorescence Microscopy* [h] *DESI-MSI: Desorption Electro Spray Mass Spectrometry Imaging (NB: 1 sample per intervention)*

[i] *HPLC results from donor and receiver compartments used as control samples in study II as well as in study III*

[j] *: Results from skin sections at 500 µm skin level used as control samples in study II as well as in study III*

chosen to investigate impact of transport kinetics on topical MTX delivery (*study III*).

Franz Skin Permeability Cells (FCs)

MTX diffused over 0.64 cm^2 skin area in FCs. MTX consisted of water-soluble MTX-disodium (Metex® aqueous solution for injection, Medac, Varberg, Sweden) in an infinite concentration of 10 mg/ml (1 w/v %, pH: 7.39) corresponding to 15.6 mg/cm^2 skin area. Stratum corneum of skin samples faced towards the donor compartment filled with 1.0 ml PBS (pH: 7.4) or MTX. Receiver compartment contained 5.5 ml PBS and a magnetic stir bar. Skin barrier impedance was measured in intact and laser-treated skin in order to ensure barrier disruption in laser-treated skin samples and intactness of control skin samples (Prep-check Electrode Impedance Meter 30Hz, General Devices, Ridgefield, New Jersey, USA). FCs were kept at 37˚C and dismounted after 21 h in *study II* and at 0.25 h, 1.5 h, 7 h, 18 h, 21 h or 24 h in *study III* (Table 4).

Detection of MTX

Intradermal and transdermal MTX concentrations were quantified by HPLC (*study II & III*), while MTX biodistribution in skin were illustrated and semi-quantified by fluorescence microscopy (*study II & III*) and supported by DESI-MSI (*study III*) (Table 4). HPLC quantification of MTX in fluids is based on fluorescence detection of irradiated MTX [89]. The MTX molecule has negligible fluorescence, while 254 nm UVC-irradiation cleaves MTX stoichiometrically to fluorescent by-products as illustrated in fig. 6 [89, 92]. In addition, this knowledge was utilized to develop a method for visualization and semi-quantification of unlabeled non-radioactive MTX biodistribution in skin sections. Fluorescence images have the potential to allow visualization as well as semi-quantification of MTX in different skin structures at various skin levels. To support the detection of MTX biodistribution in skin, a Desorption Electro-spray Ionization Mass Spectrometry Imaging (DESI-MSI) technique was adapted to visualize MTX in skin sections. DESI-MSI forms highly specific images of compounds in biological tissue sections by LC-MS and has recently been adapted to porcine skin [95].

HPLC quantification

HPLC utilizes chromatography to separate compounds dissolved in liquid solutions for identification and quantification. HPLC quantified MTX in donor fluids, receiver fluids and skin extracts of full-thickness skin or 25 µm horizontal cryo-sections (Table 4).

The HPLC system contained a binary pump and a UV-detector (Agilent Technologies 1200 series G1312B, Santa Clara, California, USA) [44, 89] and had a 100 × 2 mm Synergy Hydro-RP C18 column with 2.5 µm-particle size mounted (Phenomenex, Torrance, California, USA). The mobile phase had a flow-rate of 0.2 ml/min resulting in a retention time of 6 min. Limit of detection (LOD) was 2×10^{-5} mg/ml.

Cumulative amounts of MTX in receiver fluids and extracts from full-thickness skin were determined by HPLC in mg/ml and presented in mg/cm^2 skin surface area or percentage of applied MTX dose. MTX concentration in skin sections depended on selected skin volume determined by area × thickness and was presented as mg/cm^3 skin volume. For comparison to previous literature, results in µg/100 mg skin could be calculated based on a skin density of 1.1 g/cm^3 [96].

Fluorescence microscopy

Fluorescence microscopy enabled visualization and semi-quantitative measurements of MTX biodistribution in skin cryo-sections (Table 4). Tissue cryo-sections were illuminated 60 min at room temperature by a 254 nm UVC-lamp (Bio-Budget Technologies GmbH, Krefeld, Germany). UVC-irradiation was followed by digital fluorescence microscopy performed on a widefield fluorescence microscope (Till-Photonics/FEI GmbH, Munich, Germany) illuminated by a 150 W direct current Xenon lamp (Hamamatsu Super-Quiet, Shizuoka-ken, Japan). A dichroic mirror separated 405 nm monochromatic excitation light and 451 nm filtered emission light (Dichroic mirror: Chroma Technologies, Bellows Falls, Vermont, USA; Monochromator: PolyV, 15 nm bandwidth, Till-Photonics/FEI GmbH, Munich, Germany; Emission filter: 20 nm bandwidth, Chroma Technologies, Bellows Falls, Vermont, USA). A 12-bit gray-scale CCD camera recorded MTX-fluorescence under standardized conditions of 10 × magnification and 50 ms excita-

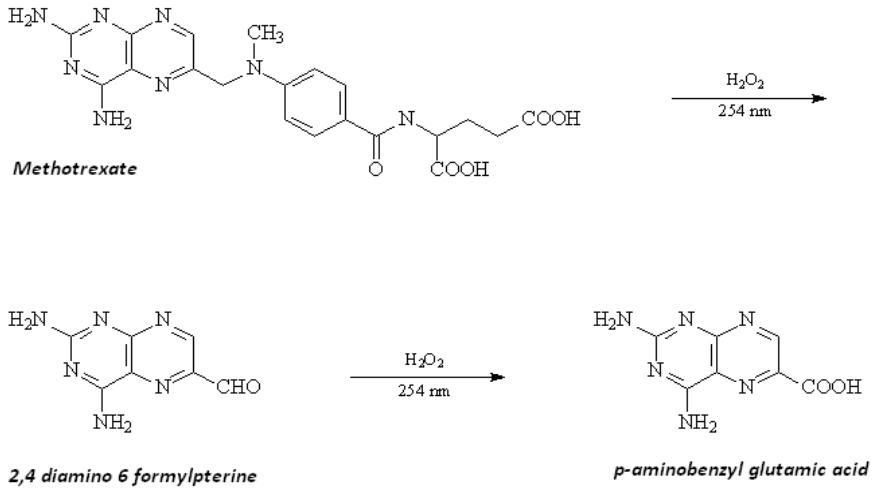

Figure 6: *Stoichiometric cleavage of Methotrexate into fluorescent bi-products by 254 nm UVC-light irradiation.*

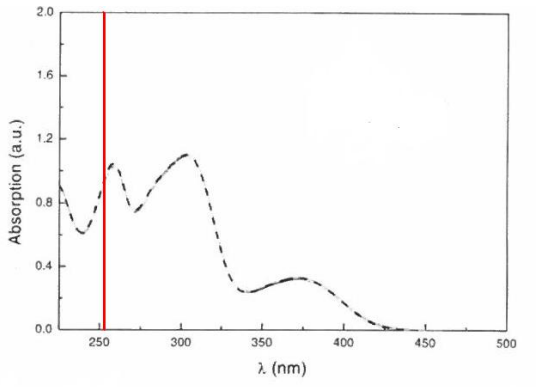

Figure 7: *Absorption spectrum of un-irradiated Methotrexate. The red line illustrates the 254 nm UVC-light applied for irradiation of MTX.. Illustration modified from Pascu et al.* [92].

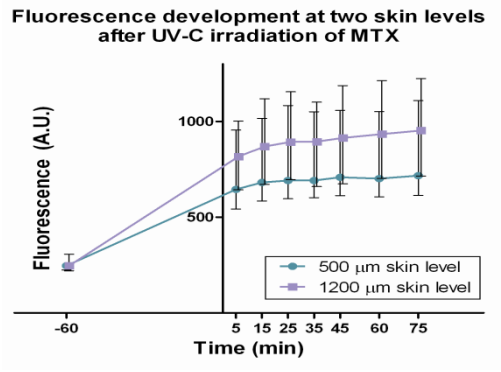

Figure 8: *Development of MTX-fluorescence after UVC-irradiation (medians, interquartile ranges). Fluorescence measured in arbitrary units (A.U.) was stable at 500 µm skin level at 35 – 75 min (p ≥ 0.060), and at 1200 µm skin level at 60 – 75 min (p=0.063). Difference in MTX-fluorescence at the two skin levels did not reach statistical difference (p≥0.310). Shown are medians and interquartile ranges.*

tion time (Hamamatsu ORCA 03, Shizuoka-ken, Japan). Image analyses were performed by a blinded evaluator in ImageJ (v. 1.47h, National Institutes of Health, Maryland, USA). Fluorescence intensities were designated in gray scale Arbitrary Units (AU). All images were assessed within a 345.000 µm^2 standardized circular area of even luminescence. The circular area had a diameter of 663 µm and distance from border of laser channel to circle circumference was up to 477 µm. Background fluorescence was measured in an empty area at the microscope slide and subtracted from measured skin values in each individual image. Porcine AFXL-processed skin had a weak autofluorescence that was detected in 21 h diffusion of PBS through AFXL-processed skin (Table 4). Individual areas of CZ and surrounding tissue were manually demarcated as regions of interest (ROIs), and fluorescence intensities were measured before and after UVC-exposure. The specific fluorescence caused by MTX was calculated by subtracting autofluorescence from MTX-images matched for intervention, ROI and UVC-exposure.

The method to detect MTX-fluorescence in skin sections was experimentally developed from pilot trials and existing literature [89, 92]. MTX-irradiation by 254 nm UVC-light was applied based on previous knowledge of the absorption spectrum for un-irradiated MTX in saline (fig. 7) [92]. To determine optimal duration of irradiation, 30, 40 and 60 min UVC irradiation was tested and the highest fluorescence intensity was seen after 60 min. In addition, small pilot tests of lamp type, irradiation distance and irradiation power were performed to optimize irradiation conditions on skin sections (data not shown).

MTX-fluorescence initially increased during the rest period after ended UVC irradiation. At 500 µm and 1200 µm skin level fluorescence intensity reached stability after 35 – 75 min (p ≥ 0.060), and 60 – 75 min (p = 0.063), respectively (fig. 8). In accordance, MTX fluorescence was standardized measured at 60 min after UVC irradiation. Excitation and emission wavelengths of 405 and 451 nm was selected for measurements of MTX-fluorescence, based on previously published excitation and emission spectra for MTX in saline (fig. 9)[92]. Possible photobleaching of MTX-fluorescence was detected as minimal under present study conditions (data not shown).

DESI-MSI

In *study III*, DESI-MSI illustrated MTX biodistribution based on the signal of *m/z* 453 for MTX (Table 4). A specific *m/z* 303 endogenous skin compound consistent with arachidonic acid was

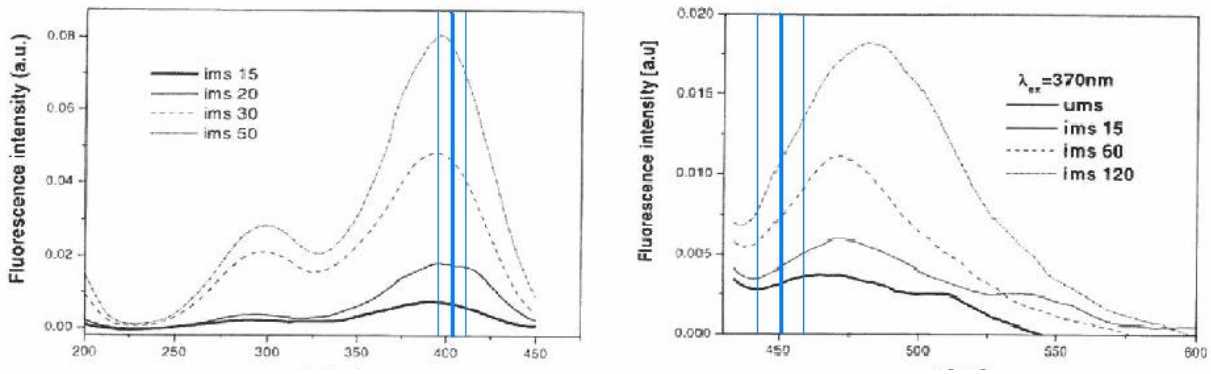

Figure 9: *Excitation and emission spectra of irradiated methotrexate in saline (ims).*
Left image: Excitation spectra after 15-50 min Xenon irradiation. Right image: Emission spectra after 15 – 120 min Xenon irradiation and 370 nm excitation. Blue lines illustrate the monochromatic excitation wavelength (15 nm bandwidth) and emission filter (20 nm bandwidth) applied in this PhD thesis. Illustration modified from Pascu et al. [92]

used as a positive control [97]. Four different interventions were analyzed consisting of MTX or PBS applied to AFXL-processed and intact control skin, respectively. Analyses were performed on a Thermo LTQ XL ion trap mass spectrometer (Thermo Fisher Scientific, San Jose, California, USA) using a custom-built DESI imaging ion source based on a motorized microscope stage (Märzhäuser, Wetzlar, Germany) [98]. Images were generated in negative ion mode with a scan range of *m/z* 150 – 1150 and processed using Biomap (Novartis, Basel, Switzerland). Additional MS/MS analyses were performed in order to confirm the presence of MTX in skin sections.

Statistics

Descriptive non-parametric statistics were used in all studies since data involved a small number of samples and Gaussian distribution could not be assumed. Statistical analyses and graphical illustrations were performed in GraphPad Prism 5 (GraphPad Software, La Jolla, CA, USA) and P values < 0.05 were considered significant. In *study I*, data consisted of medians and ranges, while in *study II* and *III*, data were described as medians and interquartile (IQ) ranges. Paired and unpaired samples were compared by Wilcoxon matched pairs and Mann-Whitney-*U* tests (2 interventions) or Friedman and Kruskal-Wallis tests (≥ 3 interventions), respectively. Bonferroni-corrections were applied to multiple comparisons.

Linear regression analyses were combined in a mathematical model in *study I* to demonstrate relationships between laser parameters and MAZ dimensions. Logarithmic transformation was performed when required to obtain linearity. Non-linear curve fittings were used in *study II* to estimate MTX concentrations and describe saturation kinetics in skin and receiver compartments.

RESULTS AND DISCUSSION

Laser-tissue interactions (*study I*)

Previous investigations

Laser-tissue interactions caused by low-powered Er:YAG AFXL are sparsely described in the literature. Previous studies evaluated histological effects of up to three stacked pulses applied with high-powered Er:YAG AFXL [21, 99]. It was demonstrated that AD increased with the total amount of energy delivered per MAZ [21, 99] as well as addition of stacked pulses and use of short pulse durations [21]. The CZ broadened by application of increased pulse energy and pulse duration [21], while impact of Er:YAG AFXL parameters on AW was not addressed.

Own investigations

Characterization of MAZs

Study I is the first to provide standardized quantitative measurements of AD, CZ and AW on a large number of histological samples generated by up to 50 repetitive stacked pulses with a miniaturized low-powered fractional Er:YAG laser. Variation of the applied laser energy generated a range of MAZ dimensions from wide superficial craters to narrow deep cone-shaped laser

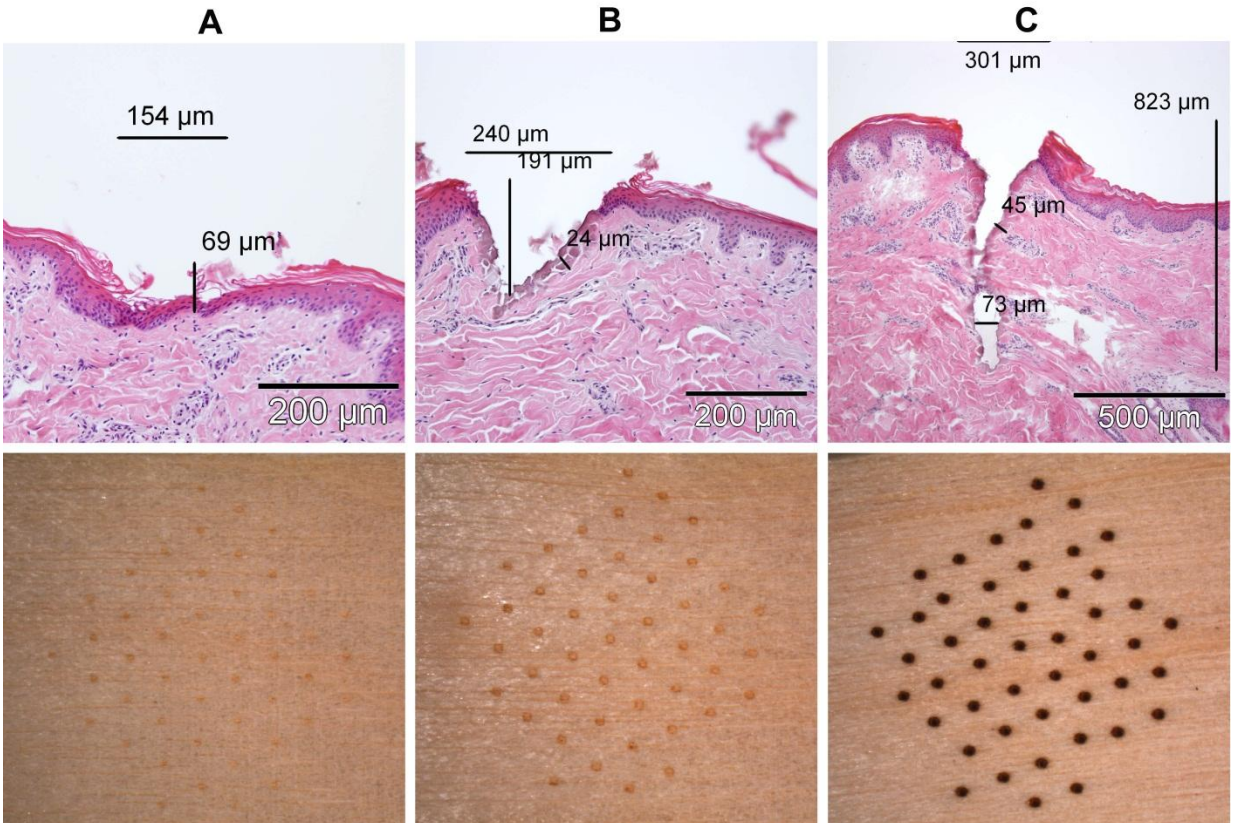

Figure 10: *Examples of MAZs generated with total energy levels of* ***A)*** *11.2mJ/MAZ,* ***B)*** *25.6 mJ/MAZ and* ***C)*** *256.0 mJ/MAZ. Top row displays single MAZs with coagulation zones and surrounding intact skin. Bottom row illustrates surface ablation of 47 MAZs/cm^2 on wooden spatulas independently of energy level. Illustration from study II.*

Table 5: Histological MAZ dimensions created by 2,940 nm fractional laser

Setting	Total Energy (mJ/MAZ)	Ablation Depth (µm) Median (Range)	Ablation Width (µm) Median (Range)	Coagulation Zone (µm) Median (Range)
0	**4.6**	NA	NA	NA
	46.0	NA	NA	NA
	115.0	192 (136 – 234)	269 (218 – 344)	56 (36 – 69)
1	**11.2**[MAZ-E]	66 (16 – 106)	177 (106 – 202)	6 (0 – 26)
	112.0	257 (179 – 317)	308 (205 – 360)	43 (32 – 60)
	280.0	431 (297 – 524)	319 (208 – 387)	66 (45 – 111)
2	**14.8**	80 (31 – 120)	131 (37 – 285)	17 (12 – 34)
	148.0	246 (106 – 347)	331 (161 – 474)	50 (35– 71)
	370.0	279 (112 – 585)	422 (227 – 488)[¤]	79 (52 – 182)
3	**25.6**[MAZ-DS]	190 (145 – 322)	154 (80 – 289)	27 (18 – 62)
	256.0[MAZ-DM]	690 (380 – 1086)	275 (94 – 414)	47 (30 – 53)
	640.0	926 (460 – 1348)[*]	371 (243 – 439)	122 (86 – 205)

[*] *Maximal obtained ablation depth* [¤] *Maximal obtained ablation width*
NA: Not Available. *Table modified from study I*
MAZ-E: 1.69 W, 11.2 mJ/MAZ, 2 stacked pulses, 5.6 mJ/pulse, 125 µs and 300 Hz
MAZ-DS: 1.28 W, 25.6 mJ/MAZ, 2 stacked pulses, 12.8 mJ/pulse, 225 µs and 100 Hz
MAZ-DM: 1.28 W, 256.0 mJ/MAZ, 20 stacked pulses, 12.8 mJ/pulse, 225 µs and 100 Hz

channels as demonstrated in fig. 10 and Table 5.

The energy threshold for creating histologically visible ablation, varied with the applied laser parameters. Thus, low pulse energy of 2.3 mJ/pulse delivered at fast pulse repetition rate required 50 stacked pulses and a total energy of 115 mJ/MAZ to produce ablation, while a higher pulse energy of 5.6 mJ/pulse delivered by lower pulse repetition rate created distinct ablation by just 2 stacked pulses and a total energy of 11.2 mJ/MAZ (Table 5, Setting 0 vs. 1).

Ablation Depth (AD)

The applied combinations of laser settings created ADs from 16 to 1348 µm (Table 5, setting 1 & 3). Depth of ablation increased linearly with the logarithm of total energy delivered per MAZ by increasing number of stacked pulses, when power, pulse energy, pulse duration, and pulse repetition rate were kept fixed (fig. 11A, $R^2 = 0.536 – 0.852$, $p < 0.001$). Maximum AD was obtained by 640.0 mJ/MAZ generated from 50 stacked pulses of 12.8 mJ/pulse (Table 5, setting 3). The deepest ablation was obtained when similar total energy was delivered by fewer stacked pulses of high pulse energy. For example, total energy of 256 mJ/MAZ achieved median AD of 690 µm by 20 stacked pulses of 12.8 mJ/pulse, while total energy of 280 mJ/MAZ generated less AD of median 431 µm by 50 stacked pulses of 5.6 mJ/pulse (Table 5, setting 3 vs. 1). The approximate depth of ablation could be estimated based on the linear relation with the logarithm of total energy: AD = slope × $\log_{10}$(Energy$_{total}$) + intercept. Slopes and intercepts varied between laser settings (setting 1: 247, -205; setting 2: 169, -121; setting 3: 523,-531) (fig. 11A).

Coagulation Zone (CZ)

Coagulation zones varied from 0 to 205 µm as presented in table 5. In superficial epidermis, MAZs presented without CZ, whereas all dermal MAZs were lined by CZ. The CZ increased linearly with total energy applied by stacked pulses ($R^2 = 0.563 – 0.753$, $p < 0.001$, fig. 11B) and could be estimated based on the linear increase: CZ = 0.17 × Energy$_{total}$ + 20 (fig. 11B). Variations in power, pulse energy, pulse duration and pulse repetition rate had minor effects on CZs but did not reach statistical significance (setting 1 – 3: $p = 0.207$, fig. 11B).

Ablation Width (AW)

Epidermal AW ranged from 37 to 488 µm, increased linearly with the logarithm of stacked pulses ($R^2 = 0.527 – 0.605$, $p < 0.001$, fig. 11C) and could be estimated based on the linear increase: AW = 138 × Log_{10}(stacks) + 123 (fig. 11C). Ablation width was minimally affected by variations in power, pulse energy, pulse duration and pulse repetition rate (setting 1 – 3: $p = 0.310$, fig. 11C).

Pulse stacking

Pulse stacking enlarged AD, CZ and AW. For example, 20 vs. 50 stacked pulses of a fixed combination of laser parameters increased median AD from 690 to 926 µm, AW from 275 to 371 µm, and CZ from 47 to 122 µm (Table 5, setting 3). Pulse stacking also increased the time used by the laser to produce each MAZ with all other laser parameters fixed; e.g. from 0.07 to 1.75 seconds by 2 vs. 50 stacked pulses of 12.8 mJ/pulse, 225 µs and 100 Hz.

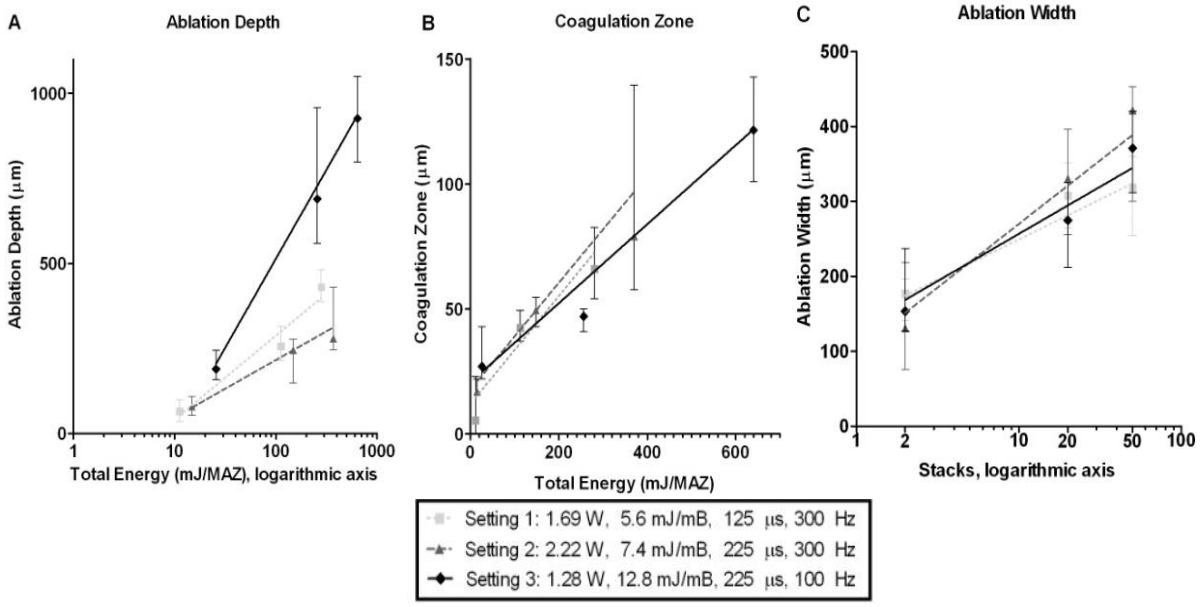

Figure 11: A) *Ablation Depth increases linearly with the logarithm of total energy: slope × $\log_{10}(Energy_{total})$ + intercept; ($p<0.001$, $R^2_1=0.852$, $R^2_2=0.536$, $R^2_3=0.748$).* ***B****) Coagulation zone increases linearly with total energy applied by stacked pulses: 0.17 × $Energy_{total}$ + 20; ($R^2_1=0.712$, $R^2_2=0.563$, $R^2_3=0.753$, $p\leq0.002$).* ***C****) Ablation width increases linearly with the logarithm of stacked pulses: 138 × Log_{10}(stacks) + 123; ($R^2_1=0.605$, $R^2_2=0.574$, $R^2_3=0.527$, $p\leq0.001$). Settings 1 and 2 were significantly different from setting 3 for ablation depth ($p < 0.001$) while differences between settings did not reach significance for ablation width and coagulation zone ($p \geq 0.207$). Illustration modified from study I.*

Table 6: Estimation of specific MAZ dimensions by mathematical modeling

	Setting 1 1.69W, 5.6 mJ/pulse, 125 µs, 300 Hz				**Setting 2 2.22 W, 7.4 mJ/pulse, 225 µs, 300 Hz**				**Setting 3 1.28 W, 12.8 mJ/pulse, 225 µs, 100 Hz**			
AD (µm)	**$Energy_{Total}$ (mJ/MAZ)**	**Stacks (#)**	**CZ (µm)**	**AW (µm)**	**$Energy_{Total}$ (mJ/MAZ)**	**Stacks (#)**	**CZ (µm)**	**AW (µm)**	**$Energy_{Total}$ (mJ/MAZ)**	**Stacks (#)**	**CZ (µm)**	**AW (µm)**
70	13	2	22	165	14	2	22	165	-	-	-	-
100	17	3	23	190	20	3	23	183	-	-	-	-
150	28	5	25	219	40	5	27	224	-	-	-	-
200	44	8	27	247	80	11	34	266	-	-	-	-
250	70	13	32	274	158	21	47	306	31	2	25	176
300	112	20	39	303	310	42	73	347	39	3	27	190
350	179	32	50	330	-	-	-	-	48	4	28	203
400	281	50	68	357	-	-	-	-	60	5	30	216
500	-	-	-	-	-	-	-	-	94	7	36	242
600	-	-	-	-	-	-	-	-	146	11	45	269
700	-	-	-	-	-	-	-	-	227	18	59	295
800	-	-	-	-	-	-	-	-	352	28	80	322
900	-	-	-	-	-	-	-	-	547	43	113	348

AD: Ablation Depth *CZ: Coagulation Zone* *AW: Ablation Width* *#: Number of stacked pulses*
MAZ: Microscopic Ablation Zone *Table from study I.*

Mathematical estimation of MAZ dimensions

According to mathematical estimations of relations between laser parameters and MAZ dimensions, *epidermal MAZs* of up to 100 µm AD could only be generated by low pulse energies of 5.6 – 7.4 mJ/pulse delivering total energy levels of 11 – 14 mJ/MAZ (fig. 11, Table 6). In *epidermal MAZs*, CZ and AW were not affected by variation in power level or pulse duration (p = 0.070, fig. 11). *Superficial dermal MAZs* of 200 to 400 µm AD could be created by total energy of 31 – 310 mJ/MAZs. All tested pulse energies (2.3 – 12.8 mJ/pulse) could create superficial dermal ablation, and AW as well as CZ varied with the applied combinations of laser parameters. For example, a MAZ of 300 µm AD had either an estimated large AW of 347 µm and thick CZ of 73 µm, or a smaller AW of 190 µm and thin CZ of 27 µm (Table 6, setting 2 and 3). *Intermediate and deep dermal MAZs* of at least 500 µm AD were only generated by the highest tested pulse energy level at applied total energy levels of 94 – 547 mJ/MAZ. For example, 352 mJ/MAZ applied by 28 stacked pulses of 12.8 mJ/pulse related to a MAZ of 800 µm AD, 80 µm CZ and 322 µm AW (Table 6, setting 3).

Discussion of results from study I

Study I adds new knowledge of laser-tissue interactions derived from a miniaturized low-powered Er:YAG laser based on large numbers of histological measurements of AD, CZ and AW. Traditional high-powered AFXLs are capable of generating high pulse energy and deliver total energy per MAZ by single or only few stacked pulses. In comparison, the low-powered devices generate less pulse energy and apply repetitive stacked pulses at the same spot in order to build up total energy delivered per MAZ, whereby pulse duration and pulse repetition rate become of increasing importance. The use of stacked pulses affects all MAZ dimensions towards enlargement of AD, CZ as well as AW. It is previously demonstrated that AD increases linearly with total energy in high-powered AFXL devices [13, 20, 21]. The same is true for the low-powered device used in present study when accumulating total energy per MAZ by stacked pulses with fixed power, pulse energy, pulse duration and pulse repetition rate. However, AD do not continue to increase linearly but follow a logarithmic curve pattern, which could be due to gradual accumulation of ablation plume interfering with incoming laser beams during the long exposure-times generated by repetitive pulse stacking. Advantages of low-powered compared to high-powered devices include small size, portability and cheaper acquisition prices, while disadvantages may be less operating stability due to the use of stacked pulses, longer exposure time, and less ability to generate deep penetration.

Impact of MAZ depth on AFXL-assisted delivery of topical MTX (*Study II*)

Previous investigations

AFXL-assisted topical MTX delivery has not previously been investigated. Thus, there is a need to investigate the importance of MAZ depth to MTX deposition and biodistribution in skin as well as transdermal permeation. However, relations between MAZ depth and drug deposition in skin has been studied *in vitro* and *in vivo* in animal models for laser-assisted topical delivery of prednisone, lidocaine, imiquimod, ingenol mebutate, MAL, ALA, and test molecules [48, 50–52, 54, 55, 61]. Results were conflicting, indicating that the impact of laser channel depth on drug deposition in skin may be affected by molecular properties of the delivered drug. Impact of MAZ depth on transdermal permeation was reported for prednisone, lidocaine, diclofenac and imiquimod in *in vitro* and *in vivo* animal models [52–54, 56], and deeper MAZs generally increased transdermal permeation of topical drugs.

Own investigations

Characterization of MAZs used for topical MTX delivery

The investigated MAZ-E, MAZ-DM and MAZ-DM were median 66, 190, and 690 µm deep; 177, 154, and 275 µm wide; and lined by 6, 27, and 47 µm of coagulation zones, respectively (fig. 10A – C). Corresponding calculated surface ablation densities were at a comparable low level of 0.9 – 2.8 % and all MAZs ablated minimal total skin volumes of 0.02 – 0.44 %.

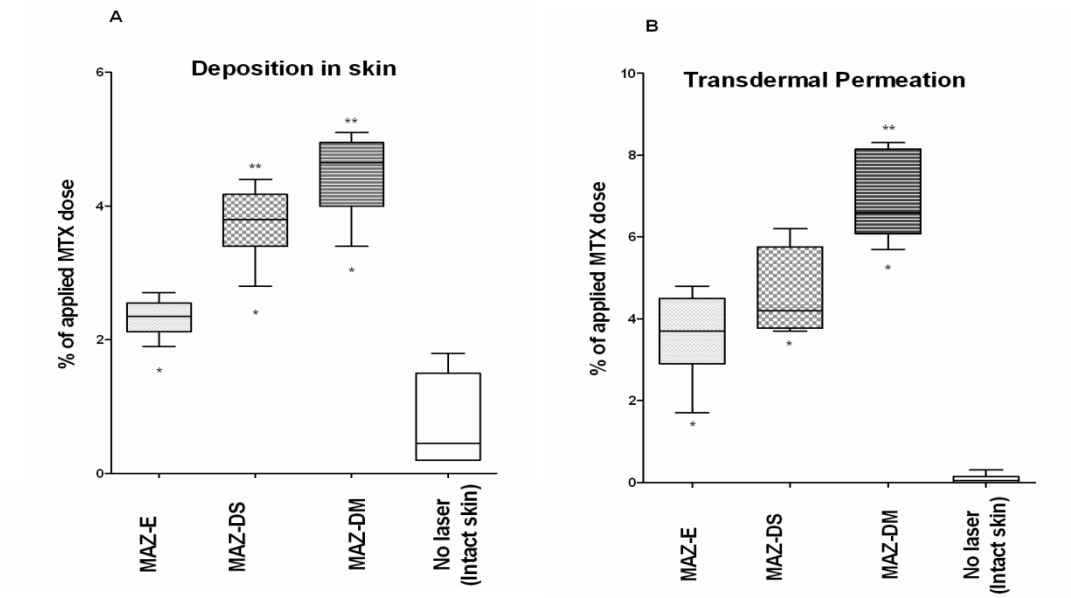

Figure 12: A) *Full-thickness skin deposition and* ***B)*** *transdermal permeation of Methotrexate (MTX) through microscopic ablation zones (MAZs) of varying depth (E: Epidermal, DS: Superfical-dermal, DM: Mid-dermal). Bonferroni-corrected by 6. *: significantly higher than intact skin, **: significantly higher than MAZ-E. Illustration from study II.*

Impact of MAZ depth on topical MTX delivery

AFXL significantly increased delivery of MTX compared to intact control skin, and the amount of MTX in skin increased by delivery through MAZs of increasing depth, confirmed quantitatively by HPLC and semi-quantitatively by fluorescence microscopy (figs. 12, 13 and 14). Thus, deposition in non-ablated full-thickness skin was 0.07 mg/cm^2 (0.45 % of 15.6 mg/cm^2 MTX applied), and increased 5-fold to 0.37 mg/cm^2 (2.37 %) by MAZ-E, 8-fold to 0.59 mg/cm^2 (3.78 %) by MAZ-DS, and 10-fold to 0.73 mg/cm^2 (4.68 %) by MAZ-DM ($p < 0.001$, fig. 12A). Transdermal permeation also increased with increasing MAZ depth (fig. 12B). Permeation through intact skin was 0.006 mg/cm^2 (0.04% of applied MTX dose), and increased 83-fold to 0.58 mg/cm^2 (3.72 %) by MAZ-E, 93-fold to 0.65 mg/cm^2 (4.17 %) by MAZ-DS and 149-fold to 1.04 mg/cm^2 (6.67 %) by MAZ-DM ($p = 0.003$, fig. 12B). The ratio of transdermal permeation versus full-thickness skin deposition varied between 1.2 and 1.7 and was independent of MAZ depth ($p = 0.172$).

Intradermal biodistribution profile of MTX

MTX was delivered by AFXL into the entire skin (figs. 13 and 14), while deeper MAZs led to delivery of more MTX at each skin layer illustrated quantitatively by HPLC ($p \leq 0.038$ at all skin levels, fig. 13) and supported semi-quantitatively by fluorescence microscopy (fig. 14, 1200 µm skin level: $p = 0.003$). MAZ-DM accumulated higher MTX-concentrations than MAZ-E throughout the skin ($p \leq 0.046$), and than MAZ-DS at 200 µm skin level ($p = 0.007$). Dermal MAZs delivered maximum MTX concentrations deeper into skin than epidermal MAZs. Thus, maximum concentration of 1.85 mg/cm^3 was delivered at 500 µm through MAZ-E, while all dermal MAZs (MAZ-DS and MAZ-DM combined) delivered maximum concentration of 3.51 mg/cm^3 at 800 µm skin level (fig. 13).

Biodistribution of MTX after saturation of coagulation zone and surrounding skin

MTX diffused radially from MAZs through CZs and was measured in up to 477 µm of surrounding skin corresponding to approximately half the distance between borders of two adjacent MAZs (fig. 10). MTX was delivered through all MAZ depths with varying CZ thicknesses; 6 µm CZ in MAZ-E, 27 µm in MAZ-DS, and 47 µm in MAZ-DM. Cross sections of MAZs were only visible at 100 and 500 µm skin levels due to the depth of the laser channels. Radial biodistribution was demonstrated by similar fluorescence intensities in CZ and surrounding skin. At 100 µm skin level, MTX-fluorescence in CZ vs. surrounding skin was 298 vs. 206 AU in MAZ-DS ($p = 0.813$) and 240 vs. 252 AU ($p = 0.438$) in MAZ-DM, while at 500 µm skin level it was 390 vs. 355 AU, ($p = 1.000$) in MAZ-DM (fig. 15).

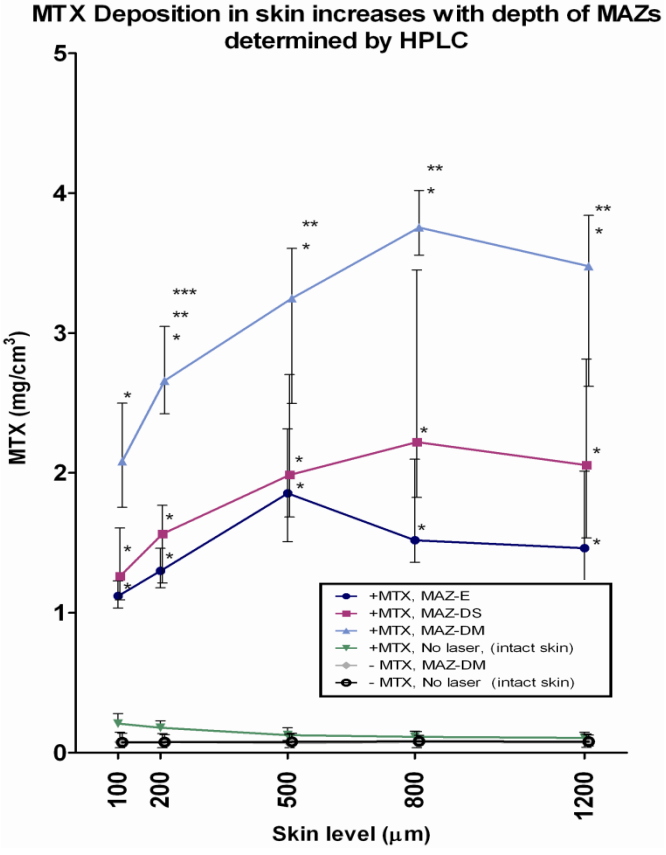

Figure 13: *HPLC quantification of skin sections from five skin levels between 100 and 1200 µm.*
: Significant compared to intact skin **: Significant compared to MAZ-E *: Significant compared to MAZ-DS. All comparisons are Bonferroni-corrected by 3.*
MAZ-E: epidermal microscopic ablation zone; MAZ-DS: Superficial dermal MAZ; MAZ-DM: mid-dermal MAZ. Illustration from study II.

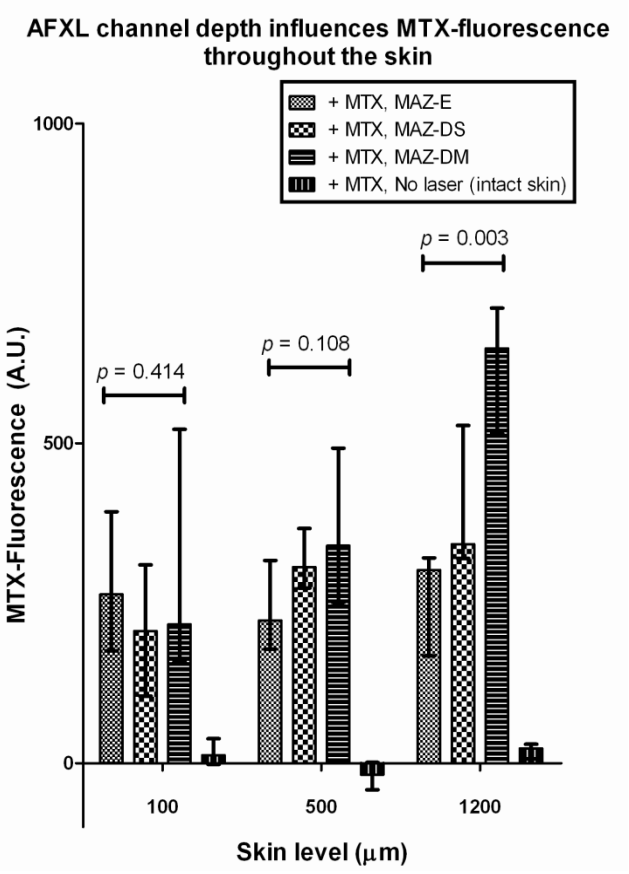

Figure 14: *Semi-quantitative measurements of fluorescence intensities in three skin levels after MTX-delivery through epidermal (MAZ-E), superficial-dermal (MAZ-DS) and mid-dermal Microscopic Ablation Zones (MAZ-DM). Values are corrected for autofluorescence. Illustration from study II.*

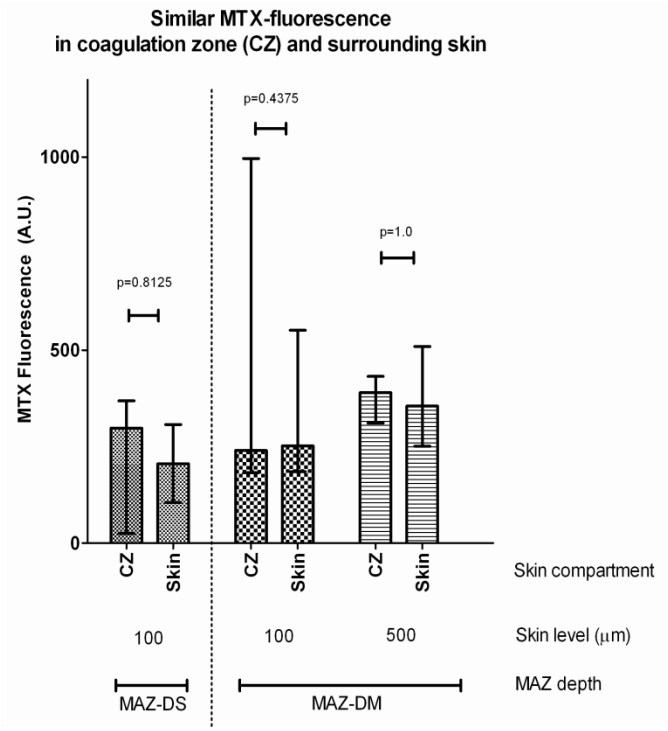

Figure 15: *Semi-quantitative measurements of Methotrexate (MTX) fluorescence in coagulation zone (CZ) and surrounding skin of superficial dermal (MAZ-DS) and mid-dermal microscopic ablation zones (MAZ-DM) at 100 µm skin level and of MAZ-DM at 500 µm skin level. All values corrected for autofluorescence. Illustration from study II.*

Discussion of results from study II

Please see study III for an overall discussion of AFXL-assisted delivery of topical MTX

Transport kinetics of AFLX-assisted topical MTX delivery (*study III*)

Previous studies

Relation between application of topical MTX on skin surface and accumulation of MTX over time within the skin is largely unknown. One previous study investigated the time perspective of topical MTX deposition by a combination of microneedles and iontophoresis in *in vivo* rat skin [72]. The skin surface was exposed to MTX for 1 h, at which time the mid-dermal MTX concentration peaked and subsequently subsided in the following 4 h [72]. Data suggest a direct proportion between topical MTX exposure and mid-dermal MTX concentration. However, results may vary with applied enhancement strategy and knowledge is lacking of biodistribution within skin and of long-term exposure in order to establish saturation kinetics and maximal level of MTX deposition in skin.

Transport kinetics of transdermal MTX permeation has previously been described *in vitro* across rodent or human skin after chemical enhancement [68, 70, 71, 104], microneedles [72, 79], iontophoresis [73–75, 77] or full-ablative laser exposure [78]. Overall,

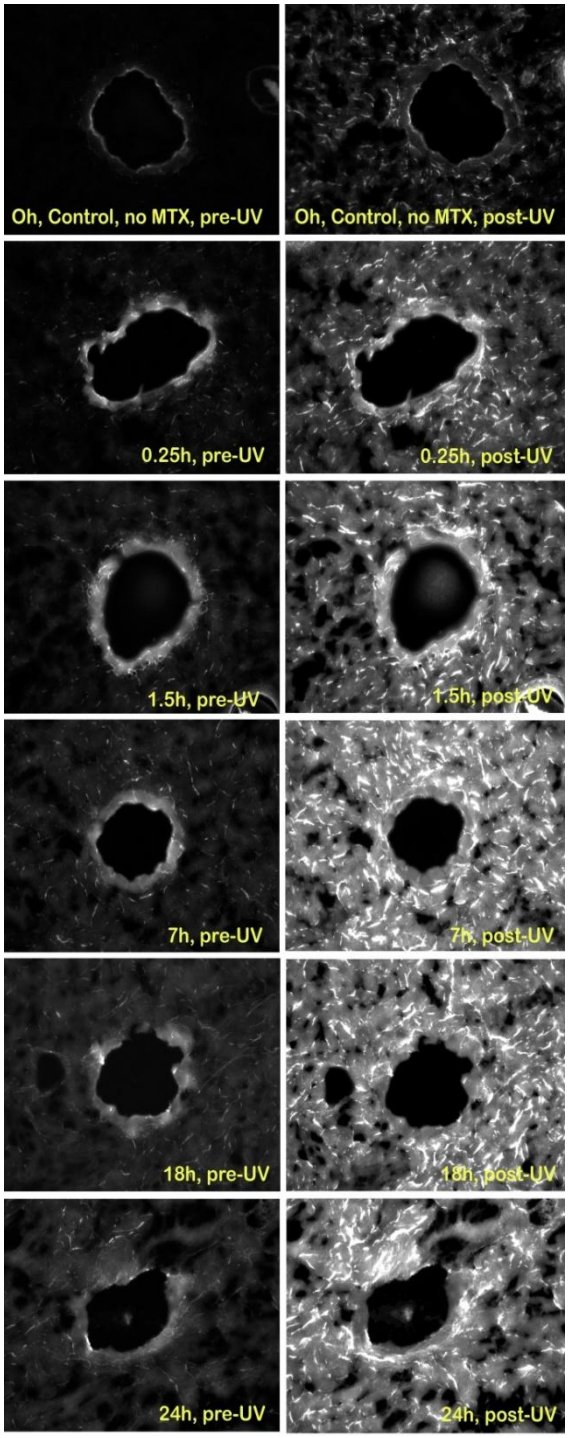

Figure 16: *Fluorescence microscopy of mid-dermal skin sections illustrating Methotrexate (MTX) delivery over time before and after UVC-activation of MTX-fluorescence. Fluorescence is homogeneously distributed apart from bright spots representing collagen cross-links* [141]. *All images are standardized displayed with grey-scale values from 195 to 1500. Illustration from study III.*

transdermal permeation was detected between 15 min and 5 h after application of MTX and increased over time up to 24- 48 h after application. The highest absorption rates were observed

shortly after application and maximal permeation was 2 – 140 times higher than passive diffusion across intact skin [68, 70–75, 77–79, 104].

Own investigations

Kinetics of MTX deposition in skin

MTX accumulated continuously over time in mid-dermal AFXL-processed skin. After 15 min of application, MTX fluorescence was visible in fluorescence microscopy images (fig. 16) and detectable by HPLC (p = 0.031, fig. 17A). Delivery for 1.5 h through AFXL-processed skin exceeded 21 h deposition in intact control skin (1.37 vs. 0.30 mg/cm^3, p = 0.002, fig. 17A) and AFXL-processed skin saturated after 7 h at a 10-fold increased concentration compared to intact control skin (3.08 vs. 0.30 mg/cm^3, p = 0.002, fig. 17A). Mathematically, MTX accumulation was estimated to fit an exponential cumulative distribution, corresponding to a physical model of transport across a permeable membrane between two compartments: MTX_{skin} (mg/cm^3) = 2.501× (1 – e $^{(-0.6022 \times time\ (h))}$), ($R^2$ = 0.788, fig. 17A). According to this mathematical estimate, mid-dermis was 50 % saturated at 1 h, 75 % saturated at 2 h, approaching complete saturation after 7 h at a predicted value of 2.50 mg/cm^3 skin volume. After 24 h diffusion, DESI-MSI illustrated that MTX had distributed in an entire mid-dermal section of AFXL-processed skin (fig. 18A). MS/MS confirmed the presence of specific MTX mass fragments in AFXL-processed skin after MTX application (fig. 18B). In contrast, MTX was not detected in intact control skin or in PBS control samples (fig. 18A vs. figs. 18C and D).

Biodistribution of MTX over time in coagulation zone and surrounding skin

MTX-fluorescence in CZ and surrounding skin increased over time as demonstrated by fluorescent images and semi-quantitative measurements (figs. 16 and 19). MTX-fluorescence in CZ increased rapidly and exceeded autofluorescence after 15 min (601 vs. 361 AU, increase: 240 AU, p = 0.015, fig. 19). In surrounding skin, MTX-fluorescence increased more slowly and reached significance compared to autofluorescence at 1.5 h (649 vs. 332 AU, increase: 317 AU, p = 0.004, fig. 19). In accordance, fluorescence intensity was higher in CZ than in surrounding skin until skin was saturated with MTX at 7 h (1.5 h: 507 vs. 317 AU (corrected for autofluorescence (cfa)), p = 0.031). After 7 h, fluorescence intensity in CZ was similar to or lower than fluorescence intensity of surrounding skin (7 h: 434 vs. 480 AU (cfa), p = 0.563, fig. 19).

Kinetics of transdermal MTX permeation

Initially, MTX permeation across AFXL-processed skin was

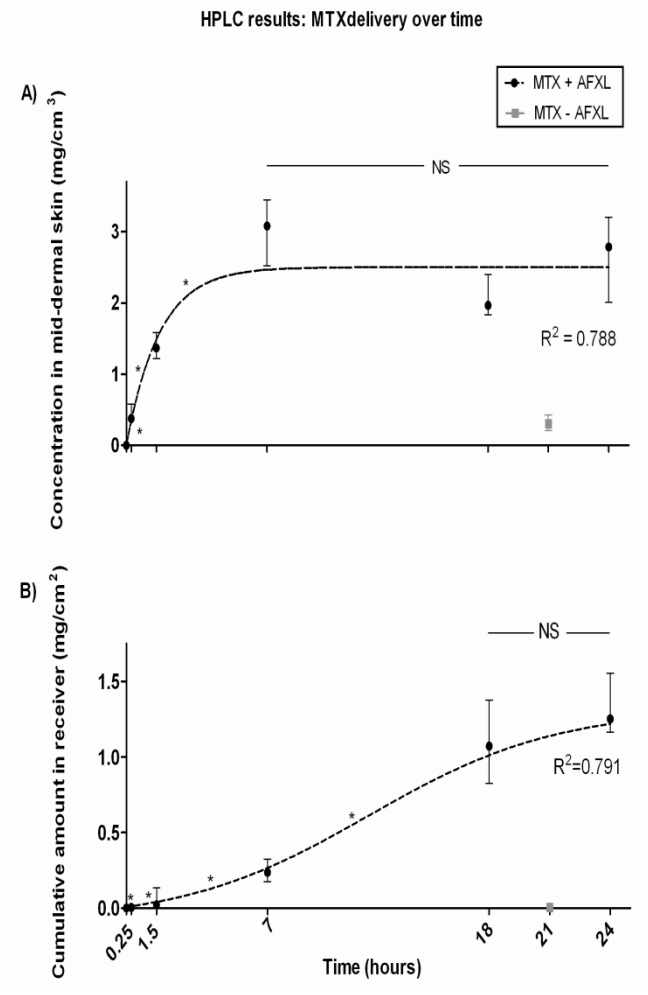

Figure 17: *Quantitative distribution over time of Methotrexate (MTX) in* ***A)*** *mid-dermal skin and* ***B)*** *receiver compartments (medians with interquartile ranges, *: p < 0.05). Illustration from study III.*

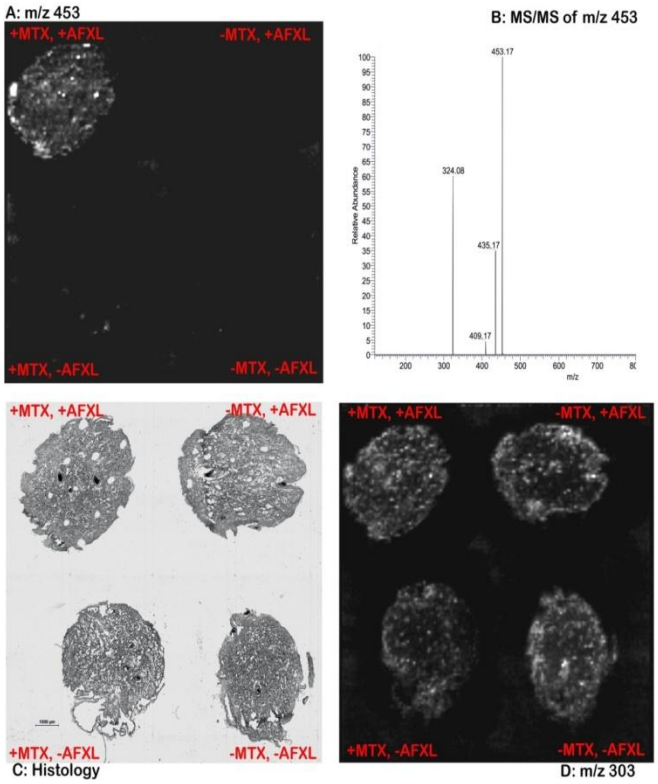

Figure 18: *Desorption Electrospray Ionization Mass Spectrometry Imaging (DESI-MSI) of mid-dermal skin sections after 24 h diffusion of methotrexate (MTX) or phosphate buffered saline (PBS) into laser-processed (+AFXL) or intact skin (-AFXL).* ***A)*** *The m/z 453 MTX-ion was present in the entire mid-dermal skin section of laser-processed skin.* ***B)*** *Tandem mass spectrometry analysis confirmed presence of specific MTX mass fragments in laser-processed skin.* ***C)*** *Histology of the four interventions was similar to* ***D)*** *DESI-MSI images of endogenous skin compound with m/z 303 that served as positive control. Illustration from study III.*

minimal. As skin was saturated by MTX at 7 h, permeation across AFXL-processed skin exceeded intact control skin (0.24 mg/cm^2 vs. 0.006 mg/cm^2, p = 0.002, fig. 17B). After skin saturation, transdermal permeation increased rapidly towards 1.25 mg/cm^2 at 24 h (8.01 % of 15.6 mg/cm^2 applied MTX), which was a 208-fold increase compared to intact control skin (1.25 mg/cm^2 vs. 0.006 mg/cm^2, p = 0.002). MTX concentration in receiver compartment was mathematically estimated based on a sigmoidal curve with nearing saturation: $MTX_{Receiver}$ (mg/cm^2) = 1.4136/ (1 + $10^{((12.04 - \text{time (h)}) \times 0.0929)}$) – 0.0936, ($R^2$ = 0.7905, fig. 17B). According to this mathematical model, receiver compartment should be 50% saturated at 13 h, 75% at 18 h, approaching a predicted saturation value of 1.32 mg/cm^2 skin surface area after 35 h.

Discussion of results (study II and III)

Pretreatment by AFXL facilitates rapid topical delivery of MTX to the skin. Regardless of MAZ depth, MTX can be found in all layers of the skin after AFXL-assisted delivery, but MAZ depth modulates total skin deposition and intradermal biodistribution within the skin layers. During the initial hours of AFXL-assisted delivery, MTX is mainly deposited in skin and the rate of absorption into surrounding skin is affected by the thermal coagulation around MAZs, while transdermal permeation is minimal. After skin saturation however, MTX is distributed to the entire skin around MAZs and the ratio of skin deposition versus transdermal permeation is constant for all MAZ depths.

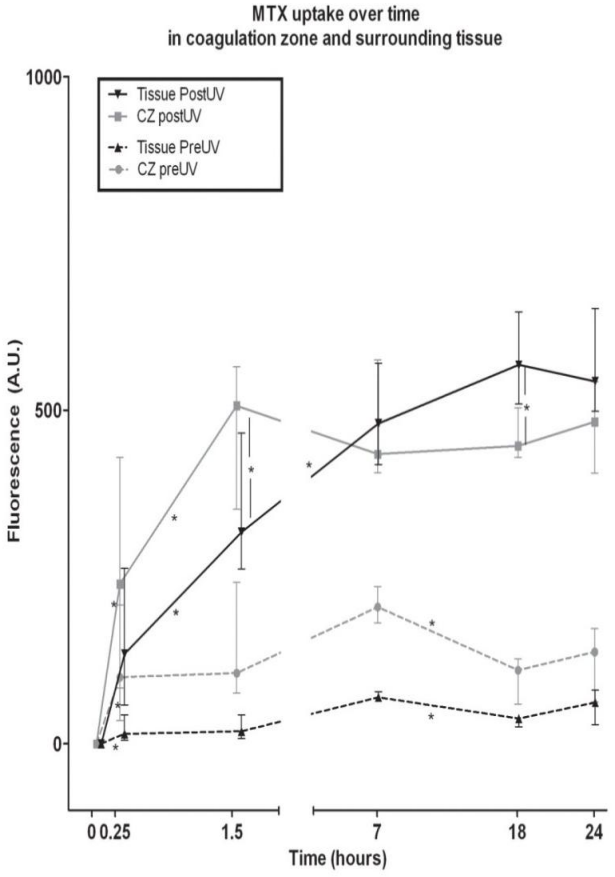

Figure 19: *Methotrexate (MTX) fluorescence over time in Coagulation zone (CZ) and surrounding mid-dermal skin. All values are corrected for autofluorescence (medians with interquartile ranges, *: p < 0.05). Illustration from study III.*

The rate of topical drug delivery into skin is determined by Fick's law of diffusion: $Flux = (P \times D \times \Delta C)/\Delta L$ [6, 7]. The partition coefficient *(P)* describes partitioning of a drug from external medium into skin at a certain concentration gradient *(ΔC)*, while diffusion through a certain distance *(ΔL)* of skin is determined by the diffusion coefficient (*D*) within skin. MTX is a *hydrophilic* molecule that diffuses negligibly through the intact lipophilic stratum corneum. Pretreatment with AFXL enables MTX delivery by disruption of skin barrier. Theoretically, the absorption rate of topical MTX is increased by reduction of *ΔL*, and by exposure of MTX to underlying skin and hydrophilic interstitial matrix with an altered *D*. In agreement, this PhD thesis demonstrated that MTX delivery through MAZ-DM for 1.5 h exceeded 21 h deposition in intact control skin. It was also demonstrated that CZ modulated the initial rate of drug absorption, which could be due to an altered *D* in the thermally coagulated tissue at the border of the ablated channels. Previously, it has been speculated whether thickness of CZ influences topical drug delivery [45]. Thermal coagulation prevents oozing and bleeding that may impair drug uptake. In contrast, CZ may in itself induce a barrier for drug uptake in the skin. Yet, a specific clinical relation between CZ and topical AFXL-assisted drug delivery is not yet established and may also be affected by molecular properties of the selected drug. The findings that biodistribution is briefly delayed by CZ, while after skin saturation MTX is distributed through CZs of 6 – 47 µm suggest that AFXL can be used for topical MTX delivery regardless of CZs although the initial rate of absorption may be affected. Thus, interesting new knowledge is added to clarify on the importance of CZs in AFXL-assisted topical delivery of hydrophilic drugs.

Present data demonstrated that delivery of hydrophilic MTX increased with MAZ depth suggesting that the stratum corneum is not the only barrier for topical drug delivery of hydrophilic molecules. However, the impact of MAZ depth on skin deposition of drug is not clearly understood in present and previous studies. Some variation of data may be caused by different laser devices, FC study designs, saturation kinetics, CZ thickness or molecular weight of applied molecules, yet none of these differences provide a clear explanation for the contradicting results [51, 53–55, 61]. However, the partition coefficient (*P*) of the diffusing drug may provide a possible explanation for the particular importance of MAZ depth to drug biodistribution in skin. The partition coefficient (*P)* covers the ratio of solubility of an un-ionized molecule in two immiscible liquids, e.g. octanol and water, while the logarithm of *P* describes *hydrophilicity* (log *P* < 0) or *lipophilicity* (log *P* > 0) of a molecule. Skin deposition of the *hydrophilic* molecules MTX (log *P* = − 1.85), sulforhodamine B (log *P* = – 0.45) [61] and methylene blue (log *P* = − 0.10) [61] increased with deeper MAZs, while accumulation of *lipophilic* molecules, e.g. prednisone (log *P* = 1.46) [54], diclofenac (log *P* = 1.90) [53], lidocaine (log *P* = 2.44) [55], and ingenol mebutate (log *P* = 2.51) [51] was not affected by MAZ depth. Interestingly, increased uptake after deeper laser penetration was not detected after AFXL-assisted delivery of photosensitizers despite the *hydrophilicity* of ALA (log *P* = −1.50) and MAL (log *P* = − 1.20) [48, 50]. However, photosensitizers are quantified by their fluorescent conversion product protoporphyrin IX (PPIX) rather than the actual amount of delivered drug. Thus, saturation of the enzymatic conversion process could be the reason why a correlation between MAZ depth and delivery of *hydrophilic* photosensitizers was not demonstrated.

In summary, AFXL facilitated rapid delivery of MTX into skin. Thermal CZ influenced the initial rate of absorption while MAZ depth modulated biodistribution within skin as well as the total

amount of delivered drug. MTX was initially deposited in skin and transdermal permeation mainly occurred after skin saturation. It was proposed that *hydrophilicity* of the MTX-molecule may be the possible explanation for the impact of MAZ depth on topical delivery.

CONCLUSIONS

This PhD thesis demonstrates that:

1. MAZ dimensions could be estimated from pre-defined combinations of laser parameters based on histological measurements and mathematical modeling of a wide range of laser-tissue interactions generated by pulse stacking with a miniaturized, low-powered Er:YAG AFXL.

2. Pre-treatment by AFXL significantly increased diffusion of topical MTX compared to intact skin. Deeper MAZs delivered higher MTX concentrations than superficial MAZs and MAZ depth influenced total skin deposition, intra-dermal biodistribution profile as well as transdermal permeation of MTX.

3. MTX absorbed rapidly into mid-dermal AFXL-processed skin and transdermal permeation was minimal until skin saturation occurred. Biodistribution of MTX to the entire surrounding skin was briefly delayed but not hindered by the thermal coagulation zones lining the laser channels.

CLINICAL PERSPECTIVES

The technique of AFXL-assisted delivery of topical MTX has the potential to replace systemic therapy of localized dermatological diseases, whereas it is less suitable for widespread or systemic disease. Laser treatment can only be applied to a limited body area due to time consumption during treatment and risk of systemic absorption of topically applied drug. Thus, potential diseases of interest include anti-tumor treatment of NMSC in specific areas or anti-inflammatory treatments of localized plaque psoriasis [105, 106], hypertrophic scars [107], granuloma annulare [108], and morphea [109]. In addition, previous investigations have demonstrated efficacy from intralesional MTX treatments of keratoacanthomas [110–116], squamous cell carcinomas [117, 118], large cell lymphomas [119, 120], cutaneous involvement of leukemia [121] and nail psoriasis [122]. Nail psoriasis can be challenging to treat [123], yet, one case report demonstrated complete clearance two years after six weekly treatments with intralesional MTX [122]. However, MTX injected directly at the nail bed is painful and requires local anaesthesia. Topical MTX delivered by AFXL may be a more convenient alternative, since AFXL-assisted drug delivery has previously been successfully applied in other nail disorders [39, 124]. Overall, the AFXL-assisted delivery of topical MTX may be a more targeted and standardized treatment compared to intralesional injections.

Potential advantages of AFXL-assisted topical delivery of MTX include targeted treatments at diseased skin in specific skin layers, enhanced local concentrations, higher efficacy, minimized adverse effects and increased compliance. However, in order to develop a successful clinical treatment from AFXL-assisted topical delivery of MTX, a number of issues need to be addressed; relevant indications should be clarified, topically applied concentrations should lead to relevant concentrations at the diseased cells, and topical MTX must be physiologically active. In addition, safety issues regarding local skin irritation and systemic absorption has to be considered.

It has been questioned whether MTX requires systemic activation or exerts local efficacy after topical application [125, 126]. Previously, chemically enhanced topical MTX application has improved psoriasis in some studies [105, 106, 127–131], yet not in others [125, 126, 132, 133]. Conflicting data may be explained by the use of various MTX concentrations and application times, or by uneven effect of chemical enhancement, which is supported by a reported range of MTX recovery in skin after chemically enhancement from 0.01% to 50% [68, 69, 71]. Within the skin, biodistribution or dispersal of MTX may vary [68, 125–127]. In addition, high concentrations of folic acid in skin may block the mechanism of action for MTX [125, 134]. Overall, literature does however support local efficacy of topical MTX in psoriasis [105, 106, 127–131] as well as in keratoacanthomas [110, 111, 113, 115, 116].

In present data, topical AFLX-assisted MTX delivery led to MTX-concentrations in mid-dermis of 168, 181 and 296 µg/100 mg skin. In comparison, MTX-concentrations of 5 or 93 µg/100 mg skin were obtained in previous studies after topical application of 2.5 mg/ml MTX by chemical enhancement [132] or intravenous injection of 82.5 mg MTX [135]. Thus, AFXL delivered higher MTX concentrations in skin than systemic administration and than previously reported chemical barrier disruption, which is likely to be clinically relevant.

Optimal concentrations of MTX to exert specific anti-tumor or anti-inflammatory activity at diseased cells in the skin must be determined. A particular clinical area of interest includes precancerous lesions and NMSC as e.g. thick actinic keratosis or nodular BCCs that can be challenging to treat [25, 32, 136, 137]. Previous investigations of cell cytotoxicity suggest that irreversible cell death is only seen after more than 18 h of MTX exposure and that re-exposure within a few days is required [44, 134, 138]. However, in order to adapt the technique of AFXL-assisted topical MTX delivery to the treatment of tumors, knowledge must be obtained from cytotoxic cell assays of varying tumor cell lines regarding optimal concentrations of MTX at the tumor cells, exposure time, effect of repetitive treatments, and treatment intervals. In addition, combination of MTX and photodynamic therapy (PDT) for the treatment of NMSC has been suggested [137, 139, 140]. Previous *in vitro* studies of tumor cell lines and *in vivo* animal studies have demonstrated that pre-treatment with low-dose systemic MTX promotes tumor cell differentiation an increases intracellular PPIX production, whereby the efficacy of PDT-treatment increases [137, 139, 140]. Thus, topical AFXL-assisted delivery of MTX followed by topical PDT seems worthy of further investigations.

The issue of safety is important when considering clinical implementation of a new AFXL-assisted topical MTX treatment. Previous *in vivo* studies found that MTX was well-tolerated topically and did not cause systemic adverse effects [105, 106, 125–130, 132, 133]. In present data, low surface ablation density of 0.9 – 2.8 % and minimal total ablation of 0.02 – 0.44 % skin volume applied for topical delivery of MTX was able to increase skin deposition up to 10-fold compared to the negligible absorption detected in intact skin. Thus, AFXL-assisted delivery of MTX may be a mild treatment causing fast recovery of skin barrier and low risk of infections and scarring. However, up to 8 % transdermal permeation of MTX was found after delivery through MAZs pene-

trating into mid-dermis. Therefore, treatment area must be limited in order to avoid clinically significant systemic absorption.

Overall, it is the clinical perspective that AFXL-assisted topical MTX-delivery may be an appropriate alternative to systemic MTX therapy for localized dermatologic disorders. Still, further investigations are needed before the technique can be translated into clinical treatments.

LIMITATIONS

The present PhD thesis represents the first investigations of AFXL-assisted delivery of topical MTX. However, data do not directly translate into clinical treatments for several reasons.

A miniaturized low-powered Er:YAG AFXL was used to generate MAZs for topical drug delivery as a general model for ablative fractional laser channels. However, small varieties may be observed in MAZs generated by different AFXL devices.

Although diffusion models, such as the FCs, are widely accepted for investigations of drug delivery, *in vitro* results may not correlate to *in vivo* data on live skin of intact blood flow and metabolism. In addition, diffusion across healthy and diseased skin may vary.

The golden standard is to use human skin for *in vitro* diffusion studies. Present data were however generated in porcine skin, since it is an acknowledged model for human skin penetration [7]. Porcine skin is frequently used in previous studies of laser-tissue interactions [20] and *in vitro* drug delivery [51, 53–55, 74], and it has previously proven anatomically, chemically and functionally similar to human skin [55, 85].

Split-thickness skin is generally recommended for studies of drug diffusion [7]. Full-thickness skin was however selected in present investigations, since potential skin barrier function of all skin layers was investigated, and MTX delivery through MAZs reaching mid-dermal skin layers could only be examined in skin of intact dermal layers.

SUMMARY

Ablative fractional lasers (AFXL) are increasingly used to treat dermatological disorders and to facilitate laser-assisted topical drug delivery. In this thesis, laser-tissue interactions generated by stacked pulses with a miniaturized low-power 2,940 nm AFXL were characterized (study I). Knowledge of the correlation between laser parameters and tissue effects was used to deliver Methotrexate (MTX) topically through microscopic ablation zones (MAZs) of precise dimensions. MTX is a well-known chemotherapeutic and anti-inflammatory drug that may cause systemic adverse effects and topical delivery is thus of potential benefit. The impact of MAZ depth (study II) and transport kinetics (study III) on MTX deposition in skin as well as transdermal permeation was determined *in vitro*. Quantitative analyses of dermal and transdermal MTX concentrations were performed by High Performance Liquid Chromatography (HPLC) (study II & III), while qualitative analyses of MTX biodistribution in skin were illustrated and semi-quantified by fluorescence microscopy (study II & III) and Desorption Electro Spray Mass Spectrometry Imaging (DESI-MSI) (study III).

Laser-tissue interactions generated by AFXL

AFXL-exposure generated a variety of MAZ-dimensions. MAZ depth increased linearly with the logarithm of total energy delivered by stacked pulses, but was also affected by variations in power, pulse energy, pulse duration, and pulse repetition rate. Coagulation zones lining MAZs increased linearly with the applied total energy, while MAZ width increased linearly with the logarithm of stacked pulses. Results were gathered in a mathematical model estimating relations between laser parameters and specific MAZ dimensions.

Impact of MAZ depth on AFXL-assisted topical MTX delivery

Pretreatment by AFXL facilitated topical MTX delivery to all skin layers. Deeper MAZs increased total MTX deposition in skin compared to superficial MAZs and altered the intra-dermal biodistribution profile towards maximum accumulation in deeper skin layers. Biodistribution of MTX occurred throughout the skin without being compromised by coagulation zones of varying thickness. The ratio of skin deposition versus transdermal permeation was constant, regardless of MAZ depth.

Impact of transport kinetics on AFXL-assisted topical MTX delivery

MTX accumulated rapidly in AFXL-processed skin. MTX was detectable in mid-dermis after 15 min and saturated the skin after 7 h at a 10-fold increased MTX-concentration compared to intact skin. Transdermal permeation stayed below 1.5 % of applied MTX before skin saturation, and increased afterwards up to 8.0 % at 24h. MTX distributed radially into the coagulation zone within 15 min of application and could be detected in surrounding skin at 1.5 h. Upon skin saturation, MTX had distributed in an entire mid-dermal skin section.

In conclusion, adjusting laser parameters and application time may enable targeted treatments of dermatological disorders and potentially pose a future alternative to systemic MTX in selected dermatological disorders.

REFERENCES

1. Warner RR, Myers MC, Taylor D a. Electron probe analysis of human skin: determination of the water concentration profile. J Invest Dermatol 1988;
2. Bouwstra J a., Ponec M. The skin barrier in healthy and diseased state. Biochim Biophys Acta - Biomembr 2006;1758:2080–2095.
3. Madison KC. Barrier function of the skin: “la raison d’etre” of the epidermis. J Invest Dermatol 2003;121:231–241.
4. Andrews SN, Jeong E, Prausnitz MR. Transdermal Delivery of Molecules is Limited by Full Epidermis, Not Just Stratum Corneum. Pharm Res 2013;30:1099–1109.
5. Kirschner N, Houdek P, Fromm M, Moll I, Brandner JM. Tight junctions form a barrier in human epidermis. Eur J Cell Biol 2010;89:839–842.
6. Bloom BS, Brauer J a, Geronemus RG. Ablative Fractional Resurfacing in Topical Drug Delivery: An Update and Outlook. Dermatol Surg 2013;839–848.
7. Kielhorn J, Melching-Kollmuss S, Mangelsdorf I. *WHO report: Dermal Absorption*. 2006.
8. Bos JD, Meinardi MM. The 500 Dalton rule for the skin penetration of chemical compounds and drugs. Exp Dermatol 2000;9:165–169.
9. Brown MB, Martin GP, Jones S a, Akomeah FK. Dermal and transdermal drug delivery systems: current and future prospects. Drug Deliv 2006;13:175–87.
10. Schuetz YB, Naik A, Guy RH, Kalia YN. Emerging strategies for the transdermal delivery of peptide and protein drugs. Expert Opin Drug Deliv 2005;2:533–548.

11. Ting WW, Vest CD, Sontheimer RD. Review of traditional and novel modalities that enhance the permeability of local therapeutics across the stratum corneum. Int J Dermatol 2004;43:538–547.
12. Lane ME. Skin penetration enhancers. Int J Pharm 2013;447:12–21.
13. Hantash BM, Bedi VP, Chan KF, Zachary CB. Ex vivo histological characterization of a novel ablative fractional resurfacing device. Lasers Surg Med 2007;39:87–95.
14. Raulin C, Karsai S, editors. *Basic Laser Physics, in: Laser and IPL Technology in Dermatology and Aesthetic Medicine*. Springer-Verlag Berlin Heidelberg 2011; 2011.
15. Parker S. Verifiable CPD paper: laser-tissue interaction. Br Dent J 2007;202:73–81.
16. Anderson RR, Parrish J a. Selective photothermolysis: precise microsurgery by selective absorption of pulsed radiation. Science 1983;220:524–527.
17. Paasch U, Haedersdal M. Laser systems for ablative fractional resurfacing. Expert Rev Med Devices 2011;8:67–83.
18. Manstein D, Herron GS, Sink RK, Tanner H, Anderson RR. Fractional photothermolysis: a new concept for cutaneous remodeling using microscopic patterns of thermal injury. Lasers Surg Med 2004;34:426–38.
19. Hantash BM, Bedi VP, Kapadia B, Rahman Z, Jiang K, Tanner H, Chan KF, Zachary CB. In vivo histological evaluation of a novel ablative fractional resurfacing device. Lasers Surg Med 2007;39:96–107.
20. Skovbølling Haak C, Illes M, Paasch U, Hædersdal M. Histological evaluation of vertical laser channels from ablative fractional resurfacing: an ex vivo pig skin model. Lasers Med Sci 2011;26:465–71.
21. Dierickx CC, Khatri K a, Tannous ZS, Childs JJ, Cohen RH, Erofeev A, Tabatadze D, Yaroslavsky I V, Altshuler GB. Micro-fractional ablative skin resurfacing with two novel erbium laser systems. Lasers Surg Med 2008;40:113–23.
22. Yoo KH, Kim BJ, Kim MN. Enhanced efficacy of photodynamic therapy with methyl 5-aminolevulinic acid in recalcitrant periungual warts after ablative carbon dioxide fractional laser: A pilot study. Dermatologic Surg 2009;35:1927–1932.
23. Kim SK, Park JY, Song HS, Kim YS, Kim YC. Photodynamic therapy with ablative carbon dioxide fractional laser for treating Bowen disease. Ann Dermatol 2013;25:335–339.
24. Braun SA, Hevezi P, Homey B, Gerber PA. Laser-assisted drug delivery: Enhanced response to ingenol mebutate after ablative fractional laser treatment. J Am Acad Dermatol 2015;72:364–365.
25. Togsverd-Bo K, Haak CS, Thaysen-Petersen D, Wulf HC, Anderson RR, Hædersdal M, Hædesdal M. Intensified photodynamic therapy of actinic keratoses with fractional CO2 laser: a randomized clinical trial. Br J Dermatol 2012;166:1262–9.
26. Helsing P, Togsverd-Bo K, Veierød MB, Mørk G, Hædersdal M. Intensified fractional CO2 laser-assisted photodynamic therapy vs. laser alone for organ transplant recipients with multiple actinic keratoses and wart-like lesions: A randomized half-side comparative trial on dorsal hands. Br J Dermatol 2013;169:1087–1092.
27. Song HS, Jung S-E, Jang YH, Kang HY, Lee E-S, Kim YC. Fractional carbon dioxide laser-assisted photodynamic therapy for patients with actinic keratosis. Photodermatol Photoimmunol Photomed 2015;n/a–n/a.doi:10.1111/phpp.12184.
28. Ko DY, Kim KH, Song KH. A randomized trial comparing methyl aminolaevulinate photodynamic therapy with and without Er:YAG ablative fractional laser treatment in Asian patients with lower extremity Bowen disease: Results from a 12-month follow-up. Br J Dermatol 2014;170:165–172.
29. Togsverd-Bo K, Lei U, Erlendsson a M, Taudorf EH, Philipsen P a, Wulf HC, Skov L, Haedersdal M. Combination of ablative fractional laser and daylight mediated photodynamic therapy for actinic keratosis in organ transplant recipients - a randomized controlled trial. Br J Dermatol 2014;467–474.
30. Lippert J, Šmucler R, Vlk M. Fractional carbon dioxide laser improves nodular basal cell carcinoma treatment with photodynamic therapy with methyl 5-aminolevulinate. Dermatologic Surg 2013;39:1202–1208.
31. Nguyen BT, Gan SD, Konnikov N, Liang C a. Treatment of superficial basal cell carcinoma and squamous cell carcinoma in situ on the trunk and extremities with ablative fractional laser-assisted delivery of topical fluorouracil. J Am Acad Dermatol 2015;72:558–560.
32. Haak CS, Togsverd-Bo K, Thaysen-Petersen D, Wulf HC, Paasch U, Anderson RR, Haedersdal M. Fractional laser-mediated photodynamic therapy of high-risk basal cell carcinomas - a randomized clinical trial. Br J Dermatol 2015;172:215–222.
33. Choi SH, Kim KH, Song K-H. Efficacy of ablative fractional laser-assisted photodynamic therapy for the treatment of actinic cheilitis: 12-month follow-up results of a prospective, randomized, comparative trial. Br J Dermatol 2015;173:184–191.
34. Choi SH, Kim KH, Song KH. Efficacy of ablative fractional laser-assisted photodynamic therapy with short-incubation time for the treatment of facial and scalp actinic keratosis: 12-month follow-up results of a randomized, prospective, comparative trial. J Eur Acad Dermatology Venereol 2015;29:1598–1605.
35. Waibel JS, Wulkan AJ, Shumaker PR. Treatment of hypertrophic scars using laser and laser assisted corticosteroid delivery. Lasers Surg Med 2013;45:135–40.
36. Cavalié M, Sillard L, Montaudié H, Bahadoran P, Lacour J. Treatment of keloids with laser-assisted topical steroid delivery : a retrospective study of 23 cases. 2015;28:74–78.
37. Rkein A, Ozog D, Waibel JS. Treatment of Atrophic Scars With Fractionated CO 2 Laser facilitating delivery of Poly-L-Lactic Acid. Dermatologic Surg 2014;40:624–631.
38. Meesters A a., Bakker MM, de Rie M a., Wolkerstorfer A. Fractional CO 2 laser assisted delivery of topical anesthetics: A randomized controlled pilot study. Lasers Surg Med 2015;Epub.
39. Lim EH, Kim HR, Park YO, Lee Y, Seo YJ, Kim CD, Lee JH, Im M. Toenail onychomycosis treated with a fractional carbon-dioxide laser and topical antifungal cream. J Am Acad Dermatol 2014;70:918–923.
40. Ma G, Wu P, Lin X, Chen H, Hu X, Jin Y, Qiu Y. Fractional carbon dioxide laser-assisted drug delivery of topical timolol solution for the treatment of deep infantile

hemangioma: A pilot study. Pediatr Dermatol 2014;31:286–291.
41. Mahmoud BH, Burnett C, Ozog D. Prospective Randomized Controlled Study to Determine the Effect of Topical Application of Botulinum Toxin A for Crow's Feet After Treatment With Ablative Fractional CO2 Laser. Dermatologic Surg 2015;41:S75–S81.
42. Ko DY, Jeon SY, Kim KH, Song KH. Fractional erbium: YAG laser-assisted photodynamic therapy for facial actinic keratoses: A randomized, comparative, prospective study. J Eur Acad Dermatology Venereol 2013;1529–1539.doi:10.1111/jdv.12334.
43. Peters G, Schornagel J, Milano G. Clinical Pharmacokinetics of Anti-metabolites. Cancer Surv 1993;17:123–156.
44. Lippens RJJ. Methotrexate. Am J Pediatr Hematol Oncol 1984;6:379–395.
45. Haedersdal M, Sakamoto FH, Farinelli W a, Doukas AG, Tam J, Anderson RR. Fractional CO(2) laser-assisted drug delivery. Lasers Surg Med 2010;42:113–22.
46. Haedersdal M, Katsnelson J, Sakamoto FH, Farinelli W a, Doukas a G, Tam J, Anderson RR. Enhanced uptake and photoactivation of topical methyl aminolevulinate after fractional CO2 laser pretreatment. Lasers Surg Med 2011;43:804–13.
47. Haedersdal M, Sakamoto FH, Farinelli WA, Doukas AG, Tam J, Anderson RR. Pretreatment with ablative fractional laser changes kinetics and biodistribution of topical 5-aminolevulinic acid (ALA) and methyl aminolevulinate (MAL). Lasers Surg Med 2014;46:462–9.
48. Haak CS, Farinelli W a, Tam J, Doukas AG, Anderson RR, Haedersdal M. Fractional laser-assisted delivery of methyl aminolevulinate: Impact of laser channel depth and incubation time. Lasers Surg Med 2012;44:787–95.
49. Lee WR, Shen SC, Pai MH, Yang HH, Yuan CY, Fang JY. Fractional laser as a tool to enhance the skin permeation of 5-aminolevulinic acid with minimal skin disruption: A comparison with conventional erbium:YAG laser. J Control Release 2010;145:124–133.
50. Forster B, Klein A, Szeimies R-M, Maisch T. Penetration enhancement of two topical 5-aminolaevulinic acid formulations for photodynamic therapy by erbium:YAG laser ablation of the stratum corneum: continuous versus fractional ablation. Exp Dermatol 2010;19:806–12.
51. Erlendsson a. M, Taudorf EH, Eriksson a. H, Haak CS, Zibert JR, Paasch U, Anderson RR, Haedersdal M. Ablative fractional laser alters biodistribution of ingenol mebutate in the skin. Arch Dermatol Res 2015;Epub.
52. Lee W-R, Shen S-C, Al-Suwayeh S a, Yang H-H, Yuan C-Y, Fang J-Y. Laser-assisted topical drug delivery by using a low-fluence fractional laser: imiquimod and macromolecules. J Control Release 2011;153:240–8.
53. Bachhav YG, Heinrich A, Kalia YN. Using laser microporation to improve transdermal delivery of diclofenac: Increasing bioavailability and the range of therapeutic applications. Eur J Pharm Biopharm 2011;78:408–14.
54. Yu J, Bachhav YG, Summer S, Heinrich a, Bragagna T, Böhler C, Kalia YN. Using controlled laser-microporation to increase transdermal delivery of prednisone. J Control Release 2010;148:e71–3.
55. Bachhav YG, Summer S, Heinrich a, Bragagna T, Böhler C, Kalia YN. Effect of controlled laser microporation on drug transport kinetics into and across the skin. J Control Release 2010;146:31–6.
56. Oni G, Brown S a, Kenkel JM. Can fractional lasers enhance transdermal absorption of topical lidocaine in an in vivo animal model? Lasers Surg Med 2012;44:168–74.
57. Koh JL, Harrison D, Swanson V, Norvell DC, Coomber DC. A comparison of laser-assisted drug delivery at two output energies for enhancing the delivery of topically applied LMX-4® cream prior to venipuncture. Anesth Analg 2007;104:847–849.
58. Hsiao CY, Huang CH, Hu S, Ko YS, Sung HC, Chen CC, Huang SY. Fractional carbon dioxide laser treatment to enhance skin permeation of ascorbic acid 2-glucoside with minimal skin disruption. Dermatologic Surg 2012;38:1284–1293.
59. Huang CH, Sung HC, Hsiao CY, Hu S, Ko YS. Transdermal delivery of three vitamin C derivatives by Er:YAG and carbon dioxide laser pretreatment. Lasers Med Sci 2013;28:807–814.
60. Hsiao C-Y, Sung H-C, Hu S, Huang C-H. Fractional CO_2 Laser Treatment to Enhance Skin Permeation of Tranexamic Acid with Minimal Skin Disruption. Dermatology 2015;230:269–275.
61. Chen X, Shah D, Kositratna G, Manstein D, Anderson RR, Wu MX. Facilitation of transcutaneous drug delivery and vaccine immunization by a safe laser technology. J Control Release 2012;159:43–51.
62. Rodriguez-Menocal L, Salgado M, Davis S, Waibel J, Shabbir A, Cox A, Badiavas E V. Percutaneous bone marrow transplantation using fractional ablative Erbium:YAG laser. PLoS One 2014;9:e93004.
63. Oni G, Lequeux C, Cho M-J, Zhang D, Lazcano E, Brown S a., Kenkel JM. Transdermal Delivery of Adipocyte-Derived Stem Cells Using a Fractional Ablative Laser. Aesthetic Surg J 2013;33:109–116.
64. Yu J, Kalaria DR, Kalia YN. Erbium:YAG fractional laser ablation for the percutaneous delivery of intact functional therapeutic antibodies. J Control Release 2011;156:53–9.
65. Pedersen T, Gluud CN, Gøtszsche PM, Wille Jørgensen PA. What is evidence-based Medicine. Ugeskr Laeger 2001;27:3769–72.
66. Outryve S Van, Schrijvers D, Brande J Van Den, Wilmes P, Bogers J, Marck E Van, Vermorken JB. Methotrexate-associated liver toxicity in a patient with breast cancer : case report and literature review. 2002;60:216–222.
67. Fang J-Y, Liu P-F, Huang C-M. Decreasing Systemic Toxicity Via Transdermal Delivery of Anticancer Drugs. Curr Drug Metab 2008;9:592–597.
68. McCullough JL, Snyder DS, Weinstein GD, Friedland A, Stein B. Factors Affecting Human Percutaneous Penetration of Methotrexate and its Analogues in Vitro. J Invest Dermatol 1976;66:103 – 107.
69. Ball MA, McCullough JL, Weinstein GD. Percutaneous Absorption of Methotrexate: Effect on Epidermal DNA Synthesis in Hairless Mice. J Invest Dermatol 1982;79:7 – 10.

70. Javadzadeh Y, Hamishehkar H. Enhancing percutaneous delivery of methotrexate using different types of surfactants. Colloids Surf B Biointerfaces 2011;82:422–6.
71. Sharma A, Arora S. Formulation and in vitro evaluation of ufasomes for dermal administration of methotrexate. ISRN Pharm 2012;2012:873653.
72. Vemulapalli V, Yang Y, Friden PM, Banga AK. Synergistic effect of iontophoresis and soluble microneedles for transdermal delivery of methotrexate. J Pharm Pharmacol 2008;60:27–33.
73. Alvarez-Figueroa MJ, Delgado-Charro MB, Blanco-Méndez J. Passive and iontophoretic transdermal penetration of methotrexate. Int J Pharm 2001;212:101–7.
74. Alvarez-Figueroa MJ, Blanco-Méndez J. Transdermal delivery of methotrexate: iontophoretic delivery from hydrogels and passive delivery from microemulsions. Int J Pharm 2001;215:57–65.
75. Prasad R, Koul V, Anand S, Khar RK. Effect of DC/mDC iontophoresis and terpenes on transdermal permeation of methotrexate: in vitro study. Int J Pharm 2007;333:70–8.
76. Prasad R, Anand S, Khar RK, Dinda AK, Koul V. Studies on in vitro and in vivo transdermal flux enhancement of methotrexate by a combinational approach in comparison to oral delivery. Drug Dev Ind Pharm 2009;35:1281–92.
77. Prasad R, Anand S, Koul V. Biophysical assessment of DC iontophoresis and current density on transdermal permeation of methotrexate. Int J Pharm Investig 2011;1:234–9.
78. Lee W-R, Shen S-C, Fang C-L, Zhuo R-Z, Fang J-Y. Topical delivery of methotrexate via skin pretreated with physical enhancement techniques: low-fluence erbium:YAG laser and electroporation. Lasers Surg Med 2008;40:468–76.
79. Abla MJ, Chaturvedula A, O'Mahony C, Banga AK. Transdermal delivery of methotrexate for pediatrics using silicon microneedles. Ther Deliv 2013;4:543–51.
80. Bronaugh RL. In vitro Percutaneous Absorption Models. Ann N Y Acad Sci 2006;188–191.doi:10.2298/ABS0901057M.
81. OECD. *OECD: Guidance document for the conduct of skin absorption studies*. 2004.
82. OECD. *OECD Guideline for the testing of chemicals. Skin absorption - in vitro Method*. 2004.
83. Sklar LR, Burnett CT, Waibel JS, Moy RL, Ozog DM. Laser assisted drug delivery: A review of an evolving technology. Lasers Surg Med 2014;46:249–62.
84. Godin B, Touitou E. Transdermal skin delivery: predictions for humans from in vivo, ex vivo and animal models. Adv Drug Deliv Rev 2007;59:1152–61.
85. Kong R, Bhargava R. Characterization of porcine skin as a model for human skin studies using infrared spectroscopic imaging. Analyst 2011;136:2359–66.
86. Barbero AM, Frasch HF. Pig and guinea pig skin as surrogates for human in vitro penetration studies: a quantitative review. Toxicol In Vitro 2009;23:1–13.
87. Sandby-Møller J, Poulsen T, Wulf HC. Epidermal thickness at different body sites: relationship to age, gender, pigmentation, blood content, skin type and smoking habits. Acta Derm Venereol 2003;83:410–3.
88. Davies DJ, Ward RJ, Heylings JR. Multi-species assessment of electrical resistance as a skin integrity marker for in vitro percutaneous absorption studies. Toxicol Vitr 2004;18:351–358.
89. Yu Z, Westerlund D, Boos K-S. Determination of methotrexate and its metabolite 7-hydroxymethotrexate by direct injection of human plasma into a column-switching liquid chromatographic system using post-column photochemical reaction with fluorimetric detection. J Chromatogr B 1997;
90. Abreu CC De, Rosa PCP, Alves BDCA, Azzalis LA, Gehrke FDS, Pereira E, Junqueira VBC, Perazzo FF, Fonseca LA. Development and validation of HPLC method to determination of Methotrexate in children oncologic patients. Eur Rev Med Pharmacol Sci 2015;19:1373–1380.
91. Wu D, Wang Y, Sun Y, Ouyang N, Qian J. A simple, rapid and reliable liquid chromatography-mass spectrometry method for determination of methotrexate in human plasma and its application to therapeutic drug monitoring. Biomed Chromatogr 2015;Epub.
92. Pascu ML, Staicu A, Voicu L, Brezeanu M, Carstocea B, Pascu R, Gazdaru D. Methotrexate as a photosensitiser. Anticancer Res 2004;24:2925–30.
93. Bachhav YG, Heinrich a., Kalia YN. Controlled intra- and transdermal protein delivery using a minimally invasive Erbium:YAG fractional laser ablation technology. Eur J Pharm Biopharm 2013;84:355–364.
94. Haak CS, Bhayana B, Farinelli WA, Anderson RR, Haedersdal M. The impact of treatment density and molecular weight for fractional laser-assisted drug delivery. J Control Release 2012;163:335–341.
95. D'Alvise J, Mortensen R, Hansen SH, Janfelt C. Detection of follicular transport of lidocaine and metabolism in adipose tissue in pig ear skin by DESI mass spectrometry imaging. Anal Bioanal Chem 2014;406:3735–42.
96. Leider M, Buncke CM. Physical dimensions of the skin. Determination of specific gravity of skin, hair and nail. Arch Dermatol 1954;69:563–569.
97. Valianpour F, Wanders RJ a, Barth PG, Overmars H, van Gennip AH. Quantitative and compositional study of cardiolipin in platelets by electrospray ionization mass spectrometry: application for the identification of Barth syndrome patients. Clin Chem 2002;48:1390–7.
98. Thunig J, Hansen SH, Janfelt C. Analysis of Secondary Plant Metabolites by Indirect Desorption Electrospray Ionization Imaging Mass Spectrometry. Anal Chem 2011;83:3256–3259.
99. Farkas JP, Richardson J a, Burrus CF, Hoopman JE, Brown S a, Kenkel JM. In vivo histopathologic comparison of the acute injury following treatment with five fractional ablative laser devices. Aesthet Surg J 2010;30:457–64.
100. Walsh JT, Flotte TJ, Deutsch TF. Er:YAG laser ablation of tissue: effect of pulse duration and tissue type on thermal damage. Lasers Surg Med 1989;9:314–26.
101. Paasch U, Bodendorf MO, Grunewald S. *Grundlagen der ablativen fraktionalen lasertherapie. In: Dermatologische Lasertherapie: Fraktionale Laser.* Berlin: KVM Verlag; 2011.
102. Stumpp OF, Bedi VP, Wyatt D, Lac D, Rahman Z, Chan KF. In vivo confocal imaging of epidermal cell migration and

dermal changes post nonablative fractional resurfacing. J Biomed Opt 2009;14:024018.
103. Paasch U, Bodendorf MO, Grunewald S. *Grundlagen der nicht ablativen fraktionalen lasertherapie. In: Dermatologische Lasertherapie: Fraktionale laser.* Berlin: KVM Verlag; 2011.
104. Lee S-W, Kim J-H, Park M-C, Park Y-B, Chae WJ, Morio T, Lee D-H, Yang S-H, Lee S-K, Lee S-K, Lee S-K. Alleviation of rheumatoid arthritis by cell-transducible methotrexate upon transcutaneous delivery. Biomaterials 2012;33:1563–72.
105. Weinstein GD, McCullough JL, Olsen E. Topical Methotrexate Therapy for Psoriasis. Arch Dermatol 1989;125:227–230.
106. Syed T a, Hadi SM, Qureshi Z a, Nordstrom CG, Ali SM. Management of psoriasis vulgaris with methotrexate 0.25% in a hydrophilic gel: a placebo-controlled, double-blind study. J Cutan Med Surg 2001;5:299–302.
107. Rabello F, Souza C, Farina Jr J. Update on hypertrophic scar treatment. Clinics 2014;69:565–573.
108. Plotner a N, Mutasim DF. Successful treatment of disseminated granuloma annulare with methotrexate. Br J Dermatol 2010;163:1123–4.
109. Koch SB, Cerci FB, Jorizzo JL, Krowchuk DP. Linear morphea: a case series with long-term follow-up of young, methotrexate-treated patients. J Dermatolog Treat 2013;24:435–8.
110. Melton JL, Nelson BR, Stough DB, Brown MD, Swanson N a., Johnson TM. Treatment of keratoacanthomas with intralesional methotrexate. J Am Acad Dermatol 1991;25:1017–1023.
111. Hurst L, Gan BS. Intralesional methotrexate in solitary keratoacanthoma. Br J Plast Surg 1995;48:243–246.
112. De Visscher JG a. M, van der Wal KGH, Blanken R, Willemse F. Treatment of giant keratoacanthoma of the skin of the lower lip with intralesional methotrexate: A case report. J Oral Maxillofac Surg 2002;60:93–95.
113. Annest NM, VanBeek MJ, Arpey CJ, Whitaker DC. Intralesional methotrexate treatment for keratoacanthoma tumors: a retrospective study and review of the literature. J Am Acad Dermatol 2007;56:989–93.
114. Martorell-Calatayud a, Requena C, Nagore E, Sanmartín O, Serra-Guillén C, Botella-Estrada R, Sanz-Motilva V, Llombart B, Alcañiz-Moscardo a, Guillén-Barona C. [Intralesional infusion of methotrexate as neoadjuvant therapy improves the cosmetic and functional results of surgery to treat keratoacanthoma: results of a randomized trial]. Actas Dermosifiliogr 2011;102:605–15.
115. Patel NP, Cervino a L. Treatment of keratoacanthoma: Is intralesional methotrexate an option? Can J Plast Surg 2011;19:e15–8.
116. Yoo MG, Kim I-H. Intralesional methotrexate for the treatment of keratoacanthoma: retrospective study and review of the korean literature. Ann Dermatol 2014;26:172–6.
117. Plascencia-Gomez A, Calderón-Rocher C, Proy-Trujillo H, Moreno-Coutiño G. Neoadjuvant intralesional methotrexate before surgery in squamous cell carcinoma. Dermatol Surg 2014;40:584–6.
118. Salido-Vallejo R, Cuevas-Asencio I, Garnacho-Sucedo G, González-Menchen a., Alcántara-Reifs C, De la Corte-Sánchez S, Vélez a., Moreno-Giménez JC. Neoadjuvant intralesional methotrexate in cutaneous squamous cell carcinoma: a comparative cohort study. J Eur Acad Dermatology Venereol 2015;n/a–n/a.doi:10.1111/jdv.13266.
119. Yokoi I, Ishikawa E, Koura A, Hosokawa Y, Tamai A, Nakai K, Moriue J, Moriue T, Yoneda K, Kubota Y. Successful treatment of primary cutaneous anaplastic large cell lymphoma with intralesional methotrexate therapy. Acta Derm Venereol 2014;94:319–20.
120. Blume JE, Stoll HL, Cheney RT. Treatment of primary cutaneous CD30+ anaplastic large cell lymphoma with intralesional methotrexate. J Am Acad Dermatol 2006;54:S229–S230.
121. Anyfantakis V, Dammak a, Wierzbicka-Hainaut E, Camus M, Osdoit S, Levilain P, Guillet G. Efficacy of intralesional methotrexate in specific cutaneous involvement of B-cell chronic lymphocytic leukaemia. J Eur Acad Dermatology Venereol 2009;24:856–856.
122. Saricaoglu H, Oz A, Turan H. Nail psoriasis successfully treated with intralesional methotrexate: Case report. Dermatology 2011;222:5–7.
123. Crowley JJ, Weinberg JM, Wu JJ, Robertson AD, Van Voorhees AS. Treatment of Nail Psoriasis. JAMA Dermatology 2015;151:87.
124. Lim E-H, Seo Y-J, Lee J-H, Im M. Onychodystrophy Treated Using Fractional Carbon Dioxide Laser Therapy and Topical Steroids: New Treatment Options for Nail Dystrophy. Dermatologic Surg 2013;39:1931–1933.
125. Comaish S, Juhlin L. Site of Action of Methotrexate in Psoriasis. Arch Dermatol 1969;100:99–106.
126. Stewart WD, Wallace SM, Runikis JO. Absorption and Local Action of Methotrexate in Human and Mouse Skin. Arch Dermatol 1972;106:357–361.
127. Sutton L, Swinehart JM, Kaplan AS, D P, Cato A. Clinical trial A clinical study to determine the efficacy and safety of 1 % methotrexate / Azone (MAZ) gel applied topically once daily in patients with psoriasis vulgaris. Int J Dermatol 2001;40:464–467.
128. Eskicirak B, Zemheri E, Cerkezoglu A. Clinical trial The treatment of psoriasis vulgaris : 1 % topical methotrexate gel. Int J Dermatol 2006;45:965–969.
129. Ali MFM, Salah M, Rafea M, Saleh N. Liposomal methotrexate hydrogel for treatment of localized psoriasis: preparation, characterization and laser targeting. Med Sci Monit 2008;14:PI66–74.
130. Fry L, MCminn RM h. Topical Methotrexate in Psoriasis. Arch Dermatol 1967;96:483–488.
131. Weinstein GD, Goldfaden G, Frost P. Methotrexate. Arch Dermatol 1971;104:236–243.
132. Bjerring P, Beck H-I, Zachariae H, Søgaard H. Topical Treatment of Psoriatic Skin with Methotrexate Cream: A Clinical, Pharmacokinetic, and Histological Study. Acta Derm Venereol 1986;66:515–519.
133. Van Scott E, Reinertson RP. Morphologic and Physiologic Effects of Chemotherapeutic Agents in Psoriasis. J Invest Dermatol 1959;33:357–369.
134. Rozenszajn L, Radnay J. The effect of Methotrexate on Transformation and Mitosis of Normal Human Blood Lymphocytes In Vitro. Blood 1974;43:401–409.
135. Liguori VR, Giglio JJ, Miller E, Sullivan RD. Effects of different dose schedules of amethopterin on serum and

tissue concentrations and urinary exretion patterns. Clin Pharmacol Ther 1962;3:34–40.
136. Good LM, Miller MD, High W a. Intralesional agents in the management of cutaneous malignancy: a review. J Am Acad Dermatol 2011;64:413–22.
137. Anand S, Ortel BJ, Pereira SP, Hasan T, Maytin E V. Biomodulatory Approaches of Photodynamic Therapy for Solid Tumors. Changes 2012;326:8–16.
138. Pinedo H, Chabner B. Role of Drug Concentration, Duration of Exposure and Endogenous Metabolites in Determining Methotrexate Cytotoxicity. Cancer Treat Rep 1977;61:709–715.
139. Anand S, Honari G, Hasan T, Elson P, Maytin E V. Low-dose methotrexate enhances aminolevulinate-based photodynamic therapy in skin carcinoma cells in vitro and in vivo. Clin Cancer Res 2009;15:3333–3343.
140. Yang D-F, Lee J-W, Chen H-M, Hsu Y-C. Topical methotrexate pretreatment enhances the therapeutic effect of topical 5-aminolevulinic acid-mediated photodynamic therapy on hamster buccal pouch precancers. J Formos Med Assoc 2014;113:591–599.
141. Gillies R, Zonios G, Anderson RR, Kollias N. Fluorescence excitation spectroscopy provides information about human skin in vivo. J Invest Dermatol 2000;115:704–7.